Resistance to PARP inhibition by DNA damage response alterations in BRCA1/2-deficient tumors

Gogola, E.

CHAPTER 6

Replication fork stability confers chemoresistance in BRCA-deficient cells

Arnab Ray Chaudhuri*, Elsa Callen*, Xia Ding, **Ewa Gogola**, Alexandra A. Duarte, Ji-Eun Lee, Nancy Wong, Vanessa Lafarga, Jennifer A. Calvo, Nicholas J. Panzarino, Sam John, Amanda Day, Anna Vidal Crespo, Binghui Shen, Linda M. Starnes, Julian R. de Ruiter, Jeremy A. Daniel, Panagiotis A. Konstantinopoulos, David Cortez, Sharon B. Cantor, Oscar Fernandez-Capetillo, Kai Ge, Jos Jonkers, Sven Rottenberg, Shyam K. Sharan & André Nussenzweig

*equal contribution

Nature. 2016; 535(7612):382-7

ABSTRACT

Cells deficient in the *Brca1* and *Brca2* genes have reduced capacity to repair DNA double-strand breaks by homologous recombination and consequently are hypersensitive to DNA-damaging agents, including cisplatin and poly(ADP-ribose) polymerase (PARP) inhibitors. Here we show that loss of the MLL3/4 complex protein, PTIP, protects *Brca1/2*-deficient cells from DNA damage and rescues the lethality of *Brca2*-deficient embryonic stem cells. However, PTIP deficiency does not restore homologous recombination activity at double-strand breaks. Instead, its absence inhibits the recruitment of the MRE11 nuclease to stalled replication forks, which in turn protects nascent DNA strands from extensive degradation. More generally, acquisition of PARP inhibitors and cisplatin resistance is associated with replication fork protection in *BRCA2*-deficient tumor cells that do not develop *BRCA2* reversion mutations. Disruption of multiple proteins, including PARP1 and CHD4, leads to the same end point of replication fork protection, highlighting the complexities by which tumor cells evade chemotherapeutic interventions and acquire drug resistance.

INTRODUCTION

The role of BRCA1 and BRCA2 in the repair of double-strand breaks (DSBs) is thought to be central to their tumor-suppressor activities, and underlies the hypersensitivity of *BRCA*-deficient cells to DNA damaging agents. While cisplatin and PARP inhibitors (PARPi) have been shown to be effective chemotherapeutic agents, most *BRCA*-mutant carcinomas acquire resistance[1]. Besides reduced uptake and increased efflux of drugs, the most well-described mechanism that drives chemotherapeutic resistance in *BRCA1/2*-deficient tumors is through the restoration of homologous recombination (HR)[1]. Identification of additional mechanisms underlying resistance to DNA damage is crucial for improving therapies and predicting tumor responses in *BRCA*-deficient cancers.

RESULTS

PTIP loss protects RFs in *Brca*-deficient cells

In addition to their roles in HR, recent studies have uncovered DSB independent functions for BRCA1 and BRCA2 during replication stress[2–6]. Since MRE11 has been implicated in mediating replication fork (RF) degradation in cell lines[2–4], we tested whether primary cells deficient in BRCA1 or BRCA2 also showed degradation of nascent replication tracts. We therefore conditionally inactivated BRCA1 and BRCA2 in B lymphocytes (*Brca1$^{f/f}$Cd19Cre; Brca2$^{f/f}$Cd19Cre*). B cells were sequentially labelled with CldU-(red) followed by IdU-(green), after which the active RFs were stalled with hydroxyurea (HU) (**Fig. 1a**). The relative shortening of the IdU tract after HU treatment serves as a measure of RF degradation (**Fig. 1a**). Upon HU treatment, wild-type (WT) cells showed a mean IdU/CldU tract ratio close to 1 (**Fig. 1b**). However, *Brca1*- and *Brca2*-deficient B cells exhibited a 30–45% reduction in the IdU tract length (**Fig. 1b–e** and **Supplementary Fig. 1a–c**). Consistent with previous data[2,3], RF degradation in B lymphocytes was dependent on MRE11 exonuclease activity (**Supplementary Fig. 1a–c**). We also tested the role of DNA2 and the Werner syndrome helicase/nuclease (WRN) in degradation of forks in *Brca2*-deficient B cells. Treatment of *Brca2* deficient cells with WRN inhibitor did not result in fork protection, whereas MRE11 and DNA2 were epistatic (**Supplementary Fig. 1c**).

Since 53BP1, RIF1, and PTIP counteract BRCA1-dependent HR by inhibiting MRE11-dependent DSB resection[7–15], we examined whether these factors might also function in RF stability. We thus inactivated BRCA1, BRCA2, RIF1, PTIP and 53BP1 in B lymphocytes (**Supplementary Fig. 2a**). Short exposure to HU did not promote significant DSB formation (**Supplementary Fig. 2b**), and fork progression rates were comparable across all genotypes (**Supplementary Fig. 2c–f**).

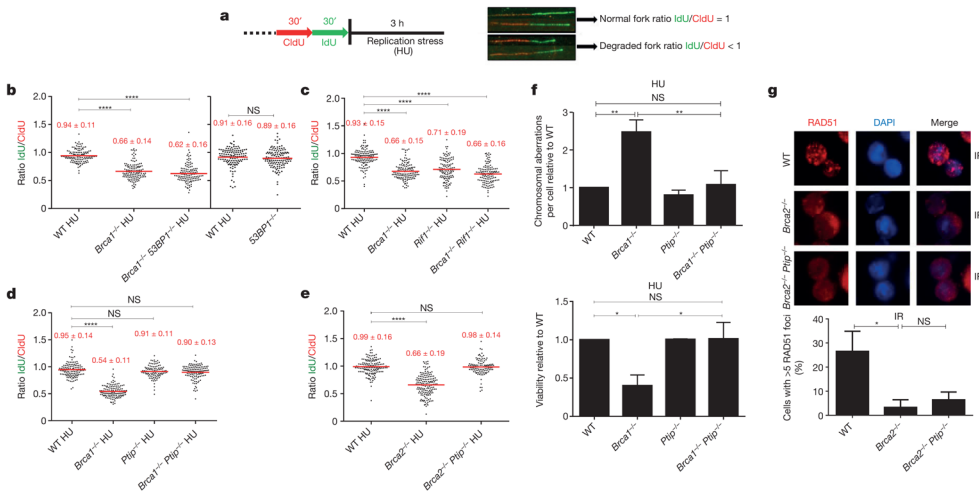

Figure 1. Loss of *Ptip* in *Brca1/2*-deficient B cells protects nascent DNA from degradation without restoring HR. **a**, Schematic for labelling B cells with CldU and IdU. **b–e**, Ratio of IdU versus CldU upon HU treatment. Numbers in red indicate the mean ± s.d. (NS, not significant, ****$P \leq 0.0001$, Mann–Whitney *U* test). One hundred and twenty-five replication forks were analysed for each genotype. **f**, Genomic instability (top) and viability upon HU treatment (bottom) relative to WT upon 6 h of 10 mM HU treatment. (**$P \leq 0.001$, *$P \leq 0.05$, unpaired *t*-test.). Fifty metaphases were analysed. **g**, Representative images (top) and quantification (below) of irradiation (IR)-induced RAD51 foci. *$P \leq 0.05$, unpaired *t*-test ($n = 120$ cells examined). Experiments were repeated three times.

Absence of 53BP1 did not protect Brca1-deficient B cells from degradation of RFs (**Fig. 1b**), consistent with the finding that BRCA1 acts in RF stabilization in a manner independent of DSB repair[2,3]. Nascent strands also shortened considerably in the absence of the 53BP1 effector *Rif1* and in *Brca1/Rif1* doubly deficient cells (**Fig. 1c**). In striking contrast, loss of *Ptip* protected RFs from HU-induced degradation in both *Brca1*- and *Brca2*-deficient cells (**Fig. 1d, e**). Moreover, while *Brca1*$^{-/-}$, *Rif1*$^{-/-}$, and *Brca1*$^{-/-}$*Rif1*$^{-/-}$ B cells displayed increased genomic instability when treated with HU (**Supplementary Fig. 3a**), *Brca1/Ptip* doubly deficient cells exhibited 2.4-fold fewer chromosomal aberrations and increased viability compared with *Brca1*$^{-/-}$ (**Fig. 1f**). Similarly, loss of *Ptip* decreased the number of chromosomal aberrations in *Brca2*$^{-/-}$ cells challenged with HU (**Supplementary Fig. 3b**), suggesting that PTIP has functions at stalled RFs distinct from its DSB-dependent interactions with 53BP1 and RIF1. We hypothesized that HU-induced degradation would impact RF progression rates. We therefore assayed the ability of WT and mutant cells to incorporate nucleotide analogues in the presence of low concentrations of HU. We observed a significant decrease in IdU tract lengths during HU exposure across all genotypes. However, *Brca2*-deficient cells had significantly decreased progression rates upon HU treatment, whereas *Ptip*$^{-/-}$ and *Brca2*$^{-/-}$*Ptip*$^{-/-}$ cells displayed significantly longer replication tracts (**Supplementary Fig. 3c**). We

also tested the effect of Ptip-deficiency on recovery after replication stalling with high concentrations of HU. We found that although the percentage of restarted RFs did not change among genotypes (**Supplementary Fig. 3d**), loss of *Brca2* resulted in a delayed restart, whereas *Brca2/Ptip* doubly deficient cells restarted normally (**Supplementary Fig. 3e**). Thus, loss of PTIP promotes RF progression and timely restart in *Brca2*-deficient cells, which correlates with decreased RF degradation.

PTIP loss rescues lethality of Brca2-null ESCs

Since elevated levels or stabilized RAD51 filaments could protect RFs from degradation[2,3,16], we asked whether PTIP deficiency leads to overexpression of RAD51 or enhanced RAD51 activity. RAD51 levels were similar in WT, $Ptip^{-/-}$, $Brca2^{-/-}$, and $Brca2^{-/-}Ptip^{-/-}$ cells (**Supplementary Fig. 3f**), but the ability of RAD51 to relocalize to sites of DNA DSBs was severely impaired in *Brca2/Ptip*-deficient B cells (**Fig. 1g and Supplementary Fig. 3g**) and embryonic stem cells (ESCs) (**Fig. 2c, d**). Moreover, loss of *Ptip* did not enhance the loading of RAD51 on nascent chromatin (**Fig. 3f**). Loss of *Brca2* in ESCs is incompatible with cell survival[17]. To test whether PTIP deficiency could promote ESC survival we knocked down PTIP in PL2F7 mouse ESCs, which have one null and one conditional allele of *Brca2* ($Brca2^{f/-}$, **Fig. 2a** and **Supplementary Fig. 4a**)[17]. After CRE transfection in $Brca2^{f/-}$ ESCs and selection in HAT medium, very few resistant colonies were obtained and these remained $Brca2^{f/-}$ rather than *Brca2*-null, reflecting the essential role of BRCA2 in ESC viability (**Fig. 2b**)[17]. Strikingly, 12.5% and 5% of the HAT-resistant colonies were *Brca2*-null when targeted by *Ptip* short hairpin RNAs (shRNAs) 1 and 2 respectively (**Fig. 2b** and **Supplementary Fig. 4b**). Consistent with our analysis of $Brca2^{-/-}Ptip^{-/-}$ B cells (**Fig. 1g**), irradiation-induced RAD51 foci formation was defective in *Brca2/Ptip*-deficient ESCs (**Fig. 2c, d**). Moreover, while efficient gene targeting to the *Pim-1* locus was observed in WT ESCs using a promoterless hygromycin cassette (100% of the hygromycin-resistant WT clones were targeted integrations), we did not observe a single targeted clone in *Brca2/Ptip*-deficient ESCs (**Fig. 2e**) indicative of defective HR. Similarly, the synthetic HR reporter substrate DR–GFP revealed impaired HR in *Brca2/Ptip*-deficient ESCs (**Supplementary Fig. 4c**). Nevertheless, stalled RFs in PTIP-deficient $Brca2^{-/-}$ ESCs displayed RF protection compared with *Brca2* hypomorphic mutant ESCs (Y3308X)[17] (**Fig. 2f**). Thus, deficiency in PTIP protects RFs from degradation and rescues the lethality of *Brca2* knockout ESCs without restoring DSB-induced HR.

BRCA2 is dispensable for HR at RFs

It has been suggested that HR at stalled forks is regulated differently from HR at DSBs[18]. As a readout for HR at RFs, we assayed for sister chromatid exchanges (SCEs) in WT and Y3308X ESCs. Although Y3308X cells show undetectable levels of irradiation-induced RAD51

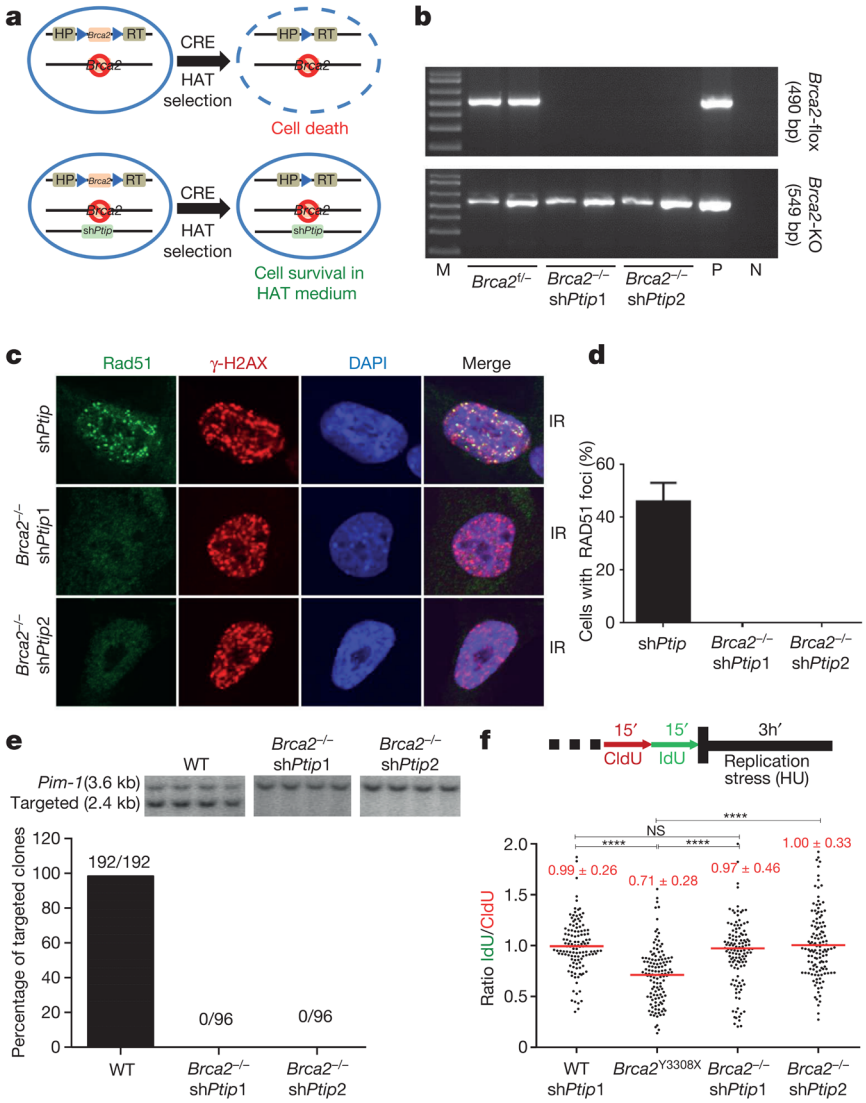

Figure 2. PTIP deficiency rescues the lethality of *Brca2*-null mouse ESCs and confers fork protection. **a**, Schematic for deletion of *Brca2*. **b**, PCR genotyping of ESC clones (M, marker; P, positive control for Brca2$^{f/-}$; N, no DNA control). **c, d**, Representative images (c) and quantification (d) of irradiation-induced foci in sh*Ptip* and Brca2$^{-/-}$/sh*Ptip* ESCs (n = 110 cells examined). **e**, Representative Southern blot images (top) and quantification for targeting efficiency (bottom) for 59xDR–GFP gene targeting to the *Pim-1* locus. **f**, Ratio of IdU versus CldU (****$P \leq 0.0001$, Mann–Whitney U test). One hundred and twenty-five replication forks were analysed.

formation and loss of targeted integration, indicative of a defect in DSB-induced HR[17], the basal frequency of SCE was normal in Y3308X cells (**Supplementary Fig. 4d**). Moreover, RAD51 was enriched on nascent DNA in Y3308X during normal replication and in presence of HU as measured by isolation of proteins on native DNA (iPOND) analysis (**Supplementary Fig. 4e**). We also observed similar frequencies of spontaneously generated and DNA damage-induced SCEs in WT, *Brca2*-null and *Brca2/Ptip*-deficient B cells (**Supplementary Fig. 4f**). Thus, in contrast to RAD51 which is required for DSB- and replication-associated HR[19], BRCA2 appears to be dispensable for HR that uses the nascent sister chromatid to repair DNA lesions during replication.

MRE11 association at RFs depends on PTIP-MLL3/4

Although the recruitment of PTIP to DSBs after irradiation is dependent on 53BP1 (**Supplementary Fig. 5a, b**)[10], we hypothesized that PTIP might be recruited to sites of stalled RFs independently of its interactions with 53BP1. Consistently, we observed PTIP accumulation at sites of replication stalling marked by pan-nuclear γ-H2AX staining[20]. Among cells exhibiting pan γ-H2AX signal, 71.4% of WT and 78% of *53bp1*$^{-/-}$ mouse embryonic fibroblasts (MEFs) exhibited PTIP foci following HU treatment (**Fig. 3a** and **Supplementary Fig. 5c**). Even in the absence of HU treatment, PTIP exhibited extensive co-localization with proliferating cell nuclear antigen (PCNA) during late S phase both in WT and in *53bp1*-deficient cells (**Fig. 3b** and **Supplementary Fig. 5d, e**). Collectively, these data suggest that PTIP might function during normal or perturbed replication in a DSB- and 53BP1-independent manner.

Like PTIP, MRE11 also associates with chromatin in a DNA damage independent but DNA replication-dependent manner[21] (**Fig. 3c**). Loss of PTIP resulted in a marked decrease of MRE11 association with PCNA foci in unperturbed cycling MEFs (**Fig. 3c**) and defective MRE11 recruitment to ssDNA regions upon HU treatment (**Supplementary Fig. 5f**). Re-introduction of WT full-length PTIP into *Ptip*$^{-/-}$ MEFs restored MRE11 co-localization with PCNA in late S phase (**Fig. 3d**). Thus, in contrast to irradiation-induced MRE11

Figure 3. PTIP localizes to sites of replication and recruits MRE1 to active and stalled replication forks. **a**, WT and *53bp1*$^{-/-}$ MEFs expressing GFP-tagged PTIP were either treated or not (NT) with 4 mM HU and assessed for γ-H2AX (red) and PTIP (green). DAPI (4′,6-diamidino-2-phenylindole) indicated in blue. Quantification in Supplementary Fig. 5c. **b**, Co-localization of PCNA (magenta) and PTIP (green). Quantification in Supplementary Fig. 5d. **c**, Co-localization of PCNA (green) and MRE11 (red). Quantification in lower panel (*n* = 150 cells examined). **d**, *Ptip*$^{-/-}$ MEFs infected with either empty vector (EV, containing IRES–GFP) or full-length PTIP (GFP–PTIP) and probed for GFP (green), MRE11 (red) and PCNA (magenta). Quantification in lower panel (*n* = 150 cells examined). **e**, MRE11 (red) and γ-H2AX (green) irradiation-induced foci. Quantification in Supplementary Fig. 5g. **f**, iPOND analyses of proteins at replication forks (capture). Input represents 0.25% of the total cellular protein content. RAD51 and MRE11 levels (shown below) were normalized to total H3. Experiments were repeated three times.

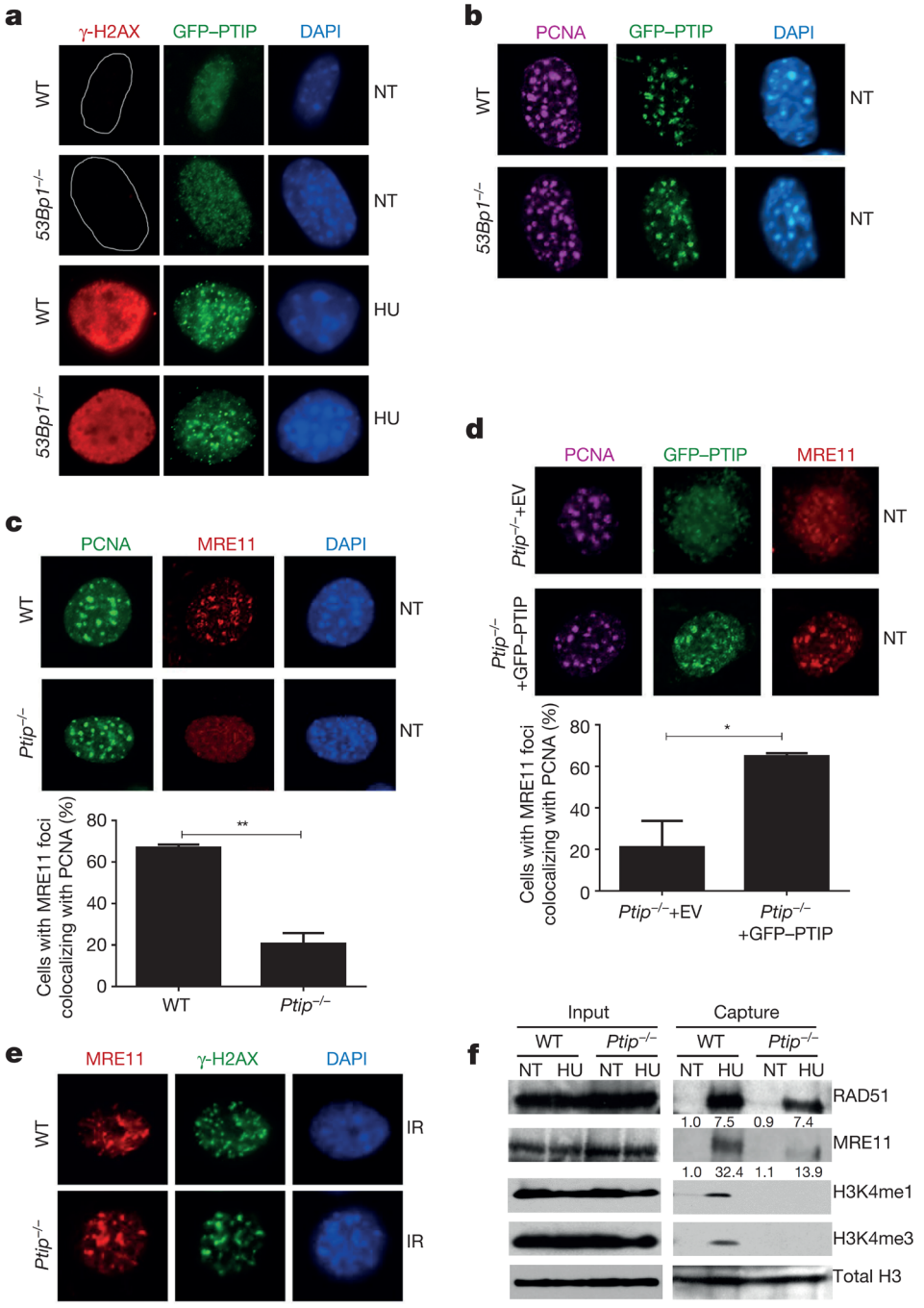
a
γ-H2AX
GFP–PTIP
DAPI
WT
NT
53Bp1−/−
NT
WT
HU
53Bp1−/−
HU
b
PCNA
GFP–PTIP
DAPI
WT
NT
53Bp1−/−
NT
c
PCNA
MRE11
DAPI
WT
NT
Ptip−/−
NT
Cells with MRE11 foci colocalizing with PCNA (%)
80
60
40
20
0
**
WT
Ptip−/−
d
PCNA
GFP–PTIP
MRE11
Ptip−/−+EV
NT
Ptip−/−
+GFP–PTIP
NT
Cells with MRE11 foci colocalizing with PCNA (%)
80
60
40
20
0
*
Ptip−/−+EV
Ptip−/−
+GFP–PTIP
e
MRE11
γ-H2AX
DAPI
WT
IR
Ptip−/−
IR
f
Input
Capture
WT
Ptip−/−
WT
Ptip−/−
NT HU NT HU
NT HU NT HU
RAD51
1.0 7.5 0.9 7.4
MRE11
1.0 32.4 1.1 13.9
H3K4me1
H3K4me3
Total H3

foci, localization of MRE11 to sites of DNA replication is PTIP-dependent (**Fig. 3c–e** and **Supplementary Fig. 5g**).

To monitor MRE11 and RAD51 association with active and stalled RFs we performed iPOND analysis in WT and *Ptip*$^{-/-}$ MEFs (**Supplementary Fig. 5h**)[22]. WT cells showed an increase in MRE11 and RAD51 association with stalled RFs (**Fig. 3f**). *Ptip*-deficient cells also showed an increase in RAD51 association at RFs, but MRE11 association with nascent DNA was reduced upon HU treatment (**Fig. 3f**), consistent with our immunofluorescence analysis (**Fig. 3c** and **Supplementary Fig. 5f**). Thus, MRE11 deposition on newly synthesized DNA is dependent on PTIP, which itself is recruited to stalled forks upon HU treatment (**Supplementary Fig. 5i**)[22].

PTIP is also known to constitutively associate with PA1 and with MLL3/MLL4 histone methyltransferases which catalyse methylation of histone H3 at lysine 4[23,24]. To identify the region of PTIP that promotes RF degradation in *Brca2*-deficient cells, we expressed EV (empty vector), FL (full-length PTIP), W165R (disrupting interactions with PA1)[25,26], W663R (disrupting interactions with 53BP1 at DSBs)[25] or Del-BRCT5-6 (disrupting interaction with MLL3/4 independently of DSBs)[23,24,26] in *Brca2/Ptip*- doubly deficient cells. We observed that only reconstitution of *Brca2/Ptip*-deficient cells with PTIP-Del-BRCT5-6 maintained fork protection (**Supplementary Fig. 6a**).

We therefore tested whether the recruitment of MRE11 at stalled forks was dependent on MLL3/4. We observed that MRE11 association at RFs was dependent on MLL3/4 as monitored by iPOND and immunofluorescence analysis (**Supplementary Fig. 6b, c**). We also observed an enrichment of H3K4me1 and H3K4me3 at nascent forks upon HU treatment that was PTIP- and MLL3/4-dependent (**Fig. 3f and Supplementary Fig. 6b**). Thus, deposition of MRE11 on newly synthesized or stalled chromatin correlates with the establishment of H3K4me1 and H3K4me3 at RFs.

To determine whether MLL4 contributes to degradation of stalled forks in *Brca*-deficient cells, we examined RF degradation in *Brca1*$^{-/-}$*Mll4*$^{-/-}$ and *Brca2*$^{-/-}$*Mll4*$^{-/-}$ B cells. *Brca1*$^{-/-}$*Mll4*$^{-/-}$ and *Brca2*$^{-/-}$*Mll4*$^{-/-}$ cells displayed a partial rescue of fork degradation (**Supplementary Fig. 6d, e**). To test whether MLL4 methyltransferase activity is critical, we targeted the catalytic SET domain of MLL4 in *Brca1*-deficient B cells. We observed a significant rescue of fork degradation in *Brca1*$^{-/-}$*Mll4*-SET$^{-/-}$ cells, suggesting that the methyltransferase activity is important for promoting fork degradation (**Supplementary Fig. 6f**).

RF protection confers chemoresistance

RF protection contributes to genome stability in a manner independent of DSB-induced HR[2,3,5]. Consistently, we observed that *Brca2*$^{-/-}$*Mll4*$^{-/-}$ B cells showed a partial rescue of chromosomal aberrations upon PARPi and cisplatin treatment compared with *Brca2*$^{-/-}$ cells alone (**Supplementary Fig. 6g**). However, *Rif1*-deficient cells, characterized by

extensive RF degradation (**Fig. 1c**) but normal irradiation-induced RAD51 foci formation (**Supplementary Fig. 7a**), showed increased chromosomal aberrations in response to replication poisons PARPi, HU and cisplatin (**Supplementary Figs 3a** and **7b, c**)[27]. We therefore speculated that RF stability mediated by loss of PTIP (**Fig. 1d, e**) might confer genome stability in *Brca*-deficient cells exposed to chemotherapeutics that poison DNA replication. Indeed, we found that *Ptip* deficiency reduced the levels of chromosomal aberrations both in *Brca1*$^{-/-}$ and in *Brca2*$^{-/-}$ B cells (**Fig. 4a, b**).

To test whether differential levels of PTIP expression could be an indicator of patient responses to platinum chemotherapy, we queried clinical information from The Cancer Genome Atlas (TCGA) of patients with *BRCA1/BRCA2*-mutated ovarian serous adenocarcinoma treated with platinum chemotherapy (**Supplementary Fig. 8a, b**). Survival analysis demonstrated that platinum-treated *BRCA2* mutants with high *PTIP* expression were correlated with a longer progression-free survival (PFS) (**Supplementary Fig. 8a**). Lower expression of *PTIP* also predicted a shorter PFS in *BRCA2*-associated ovarian cancers (**Supplementary Fig. 8b**). Taken together, these data suggest that *PTIP* levels could be a biomarker for acquired resistance to platinum-based chemotherapy in Brca1/2-mutated ovarian cancers.

An unbiased shRNA screen recently demonstrated that reduced levels of the nucleosome remodelling factor CHD4 in *BRCA2* mutant cancers correlated with poor patient response to chemotherapy, and increased tolerance to DNA-damaging agents without restoration of RAD51-dependent HR[28]. To test whether the resistance mechanism in this case occurs through RF protection, we knocked down CHD4 in the *Brca2* mutant ovarian cancer cell line PEO1 (**Supplementary Fig. 8c, d**). While CHD4 depletion in *Brca2* mutant cells did not restore HR[28], we observed that it largely conferred protection to nascent replication tracts from degradation upon HU treatment (**Fig. 4c**). Moreover, depletion of CHD4 resulted in significantly decreased recruitment of MRE11 upon HU treatment in *Brca2* mutant cells (**Supplementary Fig. 8e, f**).

These results suggest that MRE11-mediated degradation contributes to genome instability upon treatment with replication poisons. To test this idea, we pre-incubated *Brca2*-deficient B cells with the MRE11 nuclease inhibitor mirin before treating with PARP inhibitor or cisplatin. Mirin treatment did not alter the frequency of replicating cells monitored by EdU incorporation (**Supplementary Fig. 8g**). However, incubation with mirin reduced the levels of PARPi-induced chromosomal aberrations approximately two-fold. Similarly, *Brca2*-deficient cells were partly protected from cisplatin-induced DNA damage when MRE11 nuclease activity was inhibited (**Supplementary Fig. 8h**). We conclude that MRE11 nuclease promotes genomic instability in *Brca2*-deficient cells.

Since PARP1 (ARTD1) is required for MRE11 localization to stalled replication forks[29] and its loss rescues the embryonic lethality in *Brca2*-null ESCs[30], we tested the contribution

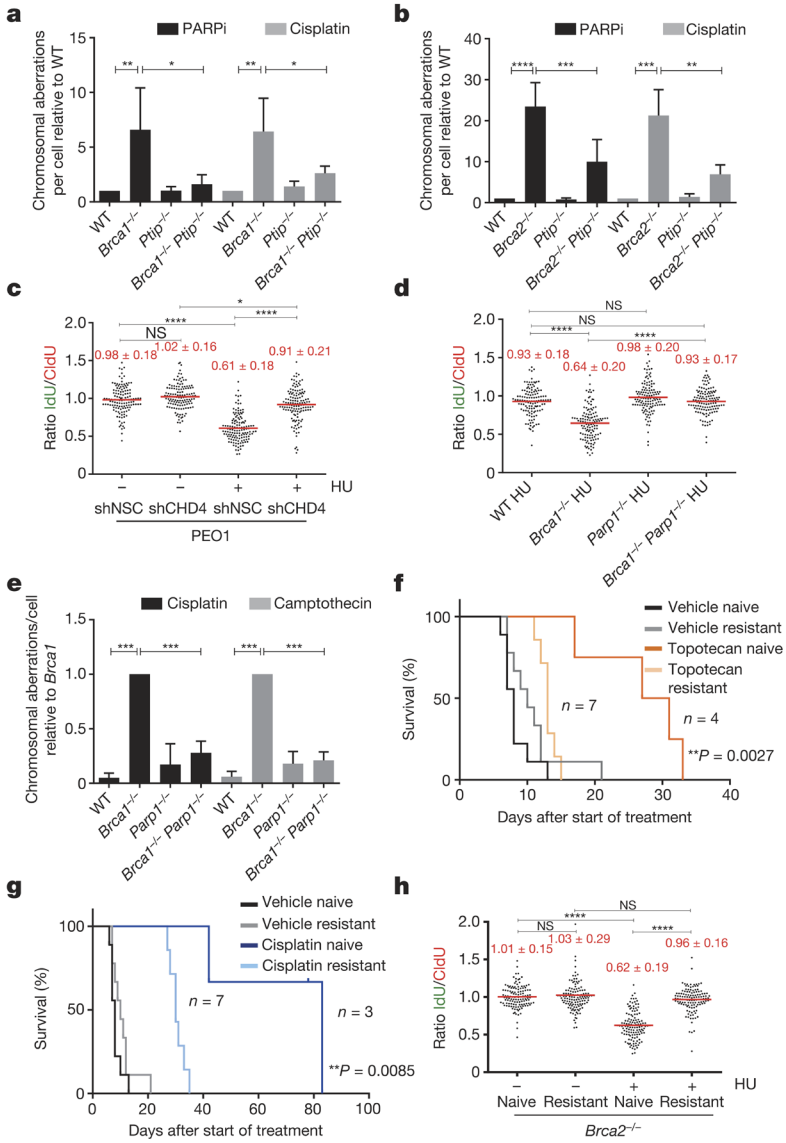

Figure 4. Replication fork protection confers genome stability and chemotherapeutic resistance. **a**, **b**, Genomic instability measured in metaphase spreads from B cells (n = 50; *$P \le 0.05$, **$P \le 0.01$, ***$P \le 0.001$, ****$P \le 0.0001$, unpaired t-test). Experiments were repeated four times. **c**, Ratio of IdU versus CldU in *Brca2*-mutated PEO1 cells either mock (shNSC) infected or infected with shRNA against CHD4 (shCHD4) (*$P \le 0.05$, ****$P \le 0.0001$, Mann–Whitney U test). One hundred and twenty-five replication forks were analysed. **d**, Ratio of IdU versus CldU in HU-treated B cells (*$P \le 0.05$, ****$P \le 0.0001$, Mann–Whitney U test). One hundred and twenty-five replication forks were analysed. **e**, Genomic instability in B cells (n = 50; ***$P \le 0.001$, unpaired t-test). Experiments repeated four times. **f**, **g**, Kaplan–Meier survival curves in mice implanted with either PARPi-naive or -resistant tumors and treated with either topotecan (f) or cisplatin (g) using log-rank (Mantel–Cox) test. **h**, Ratio of IdU versus CldU in untreated or HU-treated tumors (PARPi naive versus PARPi resistant) (****$P \le 0.0001$, Mann–Whitney U test). One hundred and twenty-five replication forks were analysed.

of PARP1 to RF stability and genome integrity by generating *Brca1*$^{-/-}$*Parp1*$^{-/-}$ B cells (*Brca1*$^{f/f}$*;Parp1*$^{-/-}$*;Cd19Cre*). Interestingly, loss of *Parp1* protected *Brca1*-deficient RFs from degradation and resulted in a significant reduction in chromosomal aberrations (**Fig. 4d, e**). Nevertheless, Parp1 deficiency failed to rescue irradiation-induced RAD51 foci formation in *Brca1*-deficient cells (**Supplementary Fig. 8i**). Thus, despite the fact that treatment with PARP inhibitor increases levels of DNA damage in *Brca1*-deficient cells[31,32], loss of *Parp1* before *Brca1* loss protects against genome instability.

To determine whether *Brca2*-deficient tumor cells acquire chemotherapy resistance via RF protection, we induced PARPi-resistance using the KB2P mouse model for *Brca2*-deficient breast cancer (**Supplementary Fig. 9a**)[33]. A mammary tumor from KB2P mice was transplanted into syngeneic FVB mice and, when the tumor reached a size >200 mm3, mice were treated with PARPi (AZD2461) for 28 consecutive days (**Supplementary Fig. 9b, c**). The tumor was initially responsive to treatment but eventually grew, upon which treatment was repeated until PARPi resistance was achieved (**Supplementary Fig. 9c**). The stability of acquired resistance was confirmed by re-transplanting matched naive and resistant tumors and treating the animals with vehicle or AZD2461 (**Supplementary Fig. 9d**). PARPi-resistant tumors also showed cross-resistance to replication poisons topotecan and cisplatin (**Fig. 4f, g**).

Both naive and resistant *Brca2*-deficient tumors showed impaired irradiation-induced RAD51 foci formation (**Supplementary Fig. 9e, f**). We therefore assayed naive and resistant tumors *ex vivo* for RF stability. The mean length of the CldU and the IdU tracts were similar in all samples that were not treated with HU (**Fig. 4h** and **Supplementary Fig. 9g**). While naive tumor cells showed degradation of nascent tracts upon HU treatment, resistant tumor cells were protected (**Fig. 4h**). These data suggest that RF protection rather than restoration of HR may be the main mechanism for acquired resistance in this mammary tumor. However, in this case, acquired resistance was not simply due to loss of PTIP or MRE11 proteins (**Supplementary Fig. 9h**).

DISCUSSION

Our study and the accompanying paper[30] provide the first examples of genetic alterations that bypass the essential requirement for DSB-induced HR, evidenced by the finding that reduction in PTIP or PARP1 (ARTD1) levels rescues the lethality of *Brca2*-null ESCs. We speculate that the reason *Brca2* nullizygosity is compatible with viability is because RAD51 is able to perform essential HR functions (such as SCE) by loading onto RFs independently of BRCA2 (**Supplementary Fig. 4e**), even if RAD51 loading onto processed DSBs is strictly dependent on BRCA2 (**Fig. 1g** and **Fig. 2c, d**). We also show that loss of PTIP, PARP1 and CHD4

confers resistance to a variety of DNA-damaging agents in BRCA-deficient cells. Resistance to PARPi and cisplatin both in primary and in tumor cells grown *in vitro* or *in vivo* correlates with protection from RF degradation. While 53BP1 disruption rescues the viability of *Brca1*-deficient mice by restoration of HR[7,9], cells from these animals show residual levels of chromosomal aberration. The significant level of RF degradation observed in *Brca1*$^{-/-}$*53bp1*$^{-/-}$ cells (**Fig. 1b**) may contribute to this genome instability.

Since RF degradation is mediated by MRE11, we propose that persistence of MRE11 at stalled forks is toxic and normally counteracted by BRCA1/2. One possibility is that MRE11 could initially be recruited to stalled forks to mediate RF restart[4], and that BRCA1/2 is necessary to subsequently disengage MRE11 from already-processed DNA termini. Consistently, we have found a significant increase in chromatin-bound MRE11 in *Brca2*-deficient cells treated with HU or cisplatin (**Supplementary Fig. 10 a, b**)[4]. In Saccharomyces cerevisiae, failure to remove MRE11 from single-stranded DNA can lead to hypersensitivity to a variety of clastogens[34,35]. We therefore propose that deficiencies in PTIP, CHD4 and PARP1 could confer drug resistance in *Brca*-deficient cells by limiting the access of MRE11 to single-strand DNA at stalled RFs.

In summary, we have shown that protection of nascent DNA from degradation provides a mechanism that can promote synthetic viability and drug resistance in *Brca*-deficient cells without restoring HR at DSBs.

ACKNOWLEDGEMENTS

We thank A. Bhandoola for discussions; K. Wolcott for flow cytometry; R. Faryabi for help with statistical analysis; T. de Lange for Rif1$^{f/f}$ mice, J. Tainer for PFM39, R. Brosh for WRNi and J. Petrini for Mre11 antibodies. This work was supported by the Intramural Research Program of the National Institutes of Health (NIH), the National Cancer Institute and the Center for Cancer Research, and by a Department of Defense grant to A.N. (BCRP DOD Idea Expansion Award, grant 11557134), and the Netherlands Organization for Scientific Research, the Dutch Cancer Society and the Swiss National Science Foundation to S.V. A.R.C. was supported by a Prospective Researcher Award from Swiss National Science Foundation (PBZHP3_147302) and Human Frontier Science Program Long-Term Fellowship (LT000393/2013). S.C. was supported by NIH grant R01 CA176166-01A1; B.S. was supported by NIH grantR01CA085344; and J.A.D. was supported by a grant to the Center for Protein Research from the Novo Nordisk Foundation (NNF14CC0001).

AUTHOR CONTRIBUTIONS

A.R.C., E.C., S.S. and A.N. conceived and planned the study. A.R.C., E.C. and X.D. designed, performed experiments and analysed data on B cells, MEFS and ESCs. E.G. and A.A.D. generated and performed experiments on PARPi-resistant tumors. J.J. and S.R. supervised the studies on PARPi-resistant tumors. N.W., A.D. and S.J. helped with experimentation. J.E.L. and K.G. generated Mll4- and Mll4-SET-deficient mice. L.S. and J.D. generated PTIP deletion constructs. B.S. provided reagents for experiments. D.C. provided advice on performing iPOND experiments and supervised iPOND mass spectrometry. J.C., N.P. and S.C. provided shCHD4 PEO1 cells and performed immunofluorescence experiments. P.K. analysed TCGA databases. V.F. and O.F.C. performed high-throughput image analysis of MRE11. S.S. supervised the ESC studies. A.R.C., E.C. and A.N. wrote the manuscript and all authors reviewed it.

Supplementary Information and source data is available in the online version of the paper (doi: 10.1038/nature18325).

REFERENCES

1. Lord, C. J. & Ashworth, A. Mechanisms of resistance to therapies targeting BRCA-mutant cancers. *Nat. Med.* **19**, 1381–1388 (2013).
2. Schlacher, K. *et al.* Double-strand break repair-independent role for BRCA2 in blocking stalled replication fork degradation by MRE11. *Cell* **145**, 529–542 (2011).
3. Schlacher, K., Wu, H. & Jasin, M. A distinct replication fork protection pathway connects Fanconi anemia tumor suppressors to RAD51-BRCA1/2. *Cancer Cell* **22**, 106–116 (2012).
4. Ying, S., Hamdy, F. C. & Helleday, T. Mre11-dependent degradation of stalled DNA replication forks is prevented by BRCA2 and PARP1. *Cancer Res.* **72**, 2814–2821 (2012).
5. Pathania, S. *et al.* BRCA1 haploinsufficiency for replication stress suppression in primary cells. *Nat Commun* **5**, 5496 (2014).
6. Pathania, S. *et al.* BRCA1 is required for postreplication repair after UV-induced DNA damage. *Mol. Cell* **44**, 235–251 (2011).
7. Bunting, S. F. *et al.* 53BP1 inhibits homologous recombination in Brca1-deficient cells by blocking resection of DNA breaks. *Cell* **141**, 243–254 (2010).
8. Bunting, S. F. *et al.* BRCA1 functions independently of homologous recombination in DNA interstrand crosslink repair. *Mol. Cell* **46**, 125–135 (2012).
9. Bouwman, P. *et al.* 53BP1 loss rescues BRCA1 deficiency and is associated with triple-negative and BRCA-mutated breast cancers. *Nat. Struct. Mol. Biol.* **17**, 688–695 (2010).
10. Callen, E. *et al.* 53BP1 mediates productive and mutagenic DNA repair through distinct phosphoprotein interactions. *Cell* **153**, 1266–1280 (2013).
11. Chapman, J. R. *et al.* RIF1 is essential for 53BP1-dependent nonhomologous end joining and suppression of DNA double-strand break resection. *Mol. Cell* **49**, 858–871 (2013).
12. Escribano-Díaz, C. *et al.* A cell cycle-dependent regulatory circuit composed of 53BP1-RIF1 and BRCA1-CtIP controls DNA repair pathway choice. *Mol. Cell* **49**, 872–883 (2013).
13. Feng, L., Fong, K.-W., Wang, J., Wang, W. & Chen, J. RIF1 counteracts BRCA1-mediated end resection during DNA repair. *J. Biol. Chem.* **288**, 11135–11143 (2013).
14. Di Virgilio, M. *et al.* Rif1 prevents resection of DNA breaks and promotes immunoglobulin class switching. *Science* **339**, 711–715 (2013).
15. Zimmermann, M., Lottersberger, F., Buonomo, S. B., Sfeir, A. & de Lange, T. 53BP1 regulates DSB repair using Rif1 to control 5' end resection. *Science* **339**, 700–704 (2013).
16. Hashimoto, Y., Ray Chaudhuri, A., Lopes, M. & Costanzo, V. Rad51 protects nascent DNA from Mre11-dependent degradation and promotes continuous DNA synthesis. *Nat. Struct. Mol. Biol.* **17**, 1305–1311 (2010).
17. Kuznetsov, S. G., Liu, P. & Sharan, S. K. Mouse embryonic stem cell-based functional assay to evaluate mutations in BRCA2. *Nat. Med.* **14**, 875–881 (2008).
18. Willis, N. A. *et al.* BRCA1 controls homologous recombination at Tus/Ter-stalled mammalian replication forks. *Nature* **510**, 556–559 (2014).
19. Sonoda, E. *et al.* Sister chromatid exchanges are mediated by homologous recombination in vertebrate cells. *Mol. Cell. Biol.* **19**, 5166–5169 (1999).
20. Toledo, L. I. *et al.* A cell-based screen identifies ATR inhibitors with synthetic lethal properties for cancer-associated mutations. *Nat. Struct. Mol. Biol.* **18**, 721–727 (2011).
21. Mirzoeva, O. K. & Petrini, J. H. J. DNA replication-dependent nuclear dynamics of the Mre11 complex. *Mol. Cancer Res.* **1**, 207–218 (2003).
22. Dungrawala, H. *et al.* The Replication Checkpoint Prevents Two Types of Fork Collapse without Regulating Replisome Stability. *Mol. Cell* **59**, 998–1010 (2015).

23. Cho, Y.-W. *et al.* PTIP associates with MLL3- and MLL4-containing histone H3 lysine 4 methyltransferase complex. *J. Biol. Chem.* **282**, 20395–20406 (2007).
24. Patel, S. R., Kim, D., Levitan, I. & Dressler, G. R. The BRCT-domain containing protein PTIP links PAX2 to a histone H3, lysine 4 methyltransferase complex. *Dev. Cell* **13**, 580–592 (2007).
25. Gong, Z., Cho, Y.-W., Kim, J.-E., Ge, K. & Chen, J. Accumulation of Pax2 transactivation domain interaction protein (PTIP) at sites of DNA breaks via RNF8-dependent pathway is required for cell survival after DNA damage. *J. Biol. Chem.* **284**, 7284–7293 (2009).
26. Starnes, L. M. *et al.* A PTIP-PA1 subcomplex promotes transcription for IgH class switching independently from the associated MLL3/MLL4 methyltransferase complex. *Genes Dev.* **30**, 149–163 (2016).
27. Buonomo, S. B. C., Wu, Y., Ferguson, D. & de Lange, T. Mammalian Rif1 contributes to replication stress survival and homology-directed repair. *J. Cell Biol.* **187**, 385–398 (2009).
28. Guillemette, S. *et al.* Resistance to therapy in BRCA2 mutant cells due to loss of the nucleosome remodeling factor CHD4. *Genes Dev.* **29**, 489–494 (2015).
29. Bryant, H. E. *et al.* PARP is activated at stalled forks to mediate Mre11-dependent replication restart and recombination. *EMBO J.* **28**, 2601–2615 (2009).
30. Ding, X. *et al.* Synthetic viability by BRCA2 and PARP1/ARTD1 deficiencies. *Nat Commun* **7**, 12425 (2016).
31. Bryant, H. E. *et al.* Specific killing of BRCA2-deficient tumours with inhibitors of poly(ADP-ribose) polymerase. *Nature* **434**, 913–917 (2005).
32. Farmer, H. *et al.* Targeting the DNA repair defect in BRCA mutant cells as a therapeutic strategy. *Nature* **434**, 917–921 (2005).
33. Jonkers, J. *et al.* Synergistic tumor suppressor activity of BRCA2 and p53 in a conditional mouse model for breast cancer. *Nat. Genet.* **29**, 418–425 (2001).
34. Chen, H. *et al.* Sae2 promotes DNA damage resistance by removing the Mre11-Rad50-Xrs2 complex from DNA and attenuating Rad53 signaling. *Proc. Natl. Acad. Sci. U.S.A.* **112**, E1880-1887 (2015).
35. Puddu, F. *et al.* Synthetic viability genomic screening defines Sae2 function in DNA repair. *EMBO J.* **34**, 1509–1522 (2015).

METHODS

Mice, MEFs, and B cell cultures.

The *53bp1*$^{-/-}$ [37], *Brca1*$^{f(\Delta 11)/f(\Delta 11)}$ (NCI mouse repository), *Brca2*$^{f/f}$ (NCI mouse repository), *Rif1f/f* [27], *Ptip*$^{f/f}$ [24] and *Mll4*$^{f/f}$ [38] mice have been described. To generate *Mll4*-SET$^{f/f}$ mice, exons 50–51 of the *Mll4/Kmt2d* gene were flanked by loxP sites. Cre-mediated deletion of the floxed exons 50–51 causes frame shift and generates a stop codon in exon 52. The resulting protein lacks the carboxy (C)-terminal 276 amino acids including the entire enzymatic SET domain. Resting splenic B cells were isolated from 8- to 12-week-old WT or mutant spleen with anti-CD43 microbeads (anti-Ly48; Miltenyi Biotech) and were cultured with LPS (25 ug/ml; Sigma), IL-4 (5 ng/ml; Sigma) and RP105 (0.5 ug/ml; BD) as described[10]. Stimulated B cells were additionally infected with CRE to ensure a high level of gene deletion in these cells. All mice were randomly distributed in experimental groups after genotyping. WT MEFs were immortalized by SV40 retroviral infection, and SV40 immortalized *Ptip*$^{f/f}$ [39] and $^{Mll3-/-}$*Mll4*$^{f/f}$ MEFs[38] were infected with a CRE retrovirus to delete *Ptip* and *Mll4* respectively. Coding sequences for mouse *Ptip*–GFP were cloned into the MIGR1 retroviral vector as previously described[10]. All cell lines used were tested for mycoplasma using a Mycoplasma Detection Kit (Invitrogen) and relevant cell lines were authenticated either by genotyping or western blot analysis. PARP inhibitor (KU58948) was obtained from AstraZeneca. Mirin was obtained from Sigma, PFM39 and WRN inhibitors were gifts from J. Tainer and R. Brosh respectively. DNA2 inhibitor has been described[40]. Cisplatin and HU were obtained from Sigma. For FISH analysis, metaphases were prepared and imaged as described10. Animal experiments were approved by the Animal Care and Use Committee of NCI-Bethesda and the Animal Ethical Committee of The Netherlands Cancer Institute.

Generation of CHD4-deficient PEO1 lines using RNAi.

BRCA2-mutated ovarian cancer cell lines PEO1 were grown in DMEM with 10% FBS and 1% Glutmax. RNAi for CHD4 was performed as previously described[28].

ESC lines, shRNA knockdowns and rescue of BRCA2 viability.

PL2F2 mouse ESCs were maintained in M15 media (Knockout DMEM with 15% fetal bovine serum, 0.00072% β-mercaptoethanol, 100 U/ml penicillin, 100 ug/ml streptomycin and 0.292 mg/ml l-glutamine) at 37 °C, 5% CO2. ESCs were plated on a monolayer of mitotically inactive feeder cells as described previously[17]. BRCA2 conditional knockout ESCs were generated as previously described[17]. Two different shRNAs against *Ptip* mRNA were cloned into pSuperior vector (Oligoengine). shRNA sequences are listed below with the targeted sequences underlined: m*Ptip* shRNA-1 sense, 5′GATCCCC GTGGCGCTCTCCTGCCAGT TTCAAGAGA ACTGGCAGGAGAGCGCCAC TTTTTA 3′; m*Ptip* shRNA-1 antisense, 5′

AGCTTAAAAA GTGGCGCTCTCCTGCCAGT TCTCTTGAA ACTGGCAGGAGAGCGCCAC GGG 3′; m*Ptip* shRNA-2 sense, 5′GATCCCC CCGTAGCAACACAGTCCTC TTCAAGAGA GAGGACTGTGTTGCTACGG TTTTTA 3′; m*Ptip* shRNA-2 antisense, 5′ AGCTTAAAAA CCGTAGCAACACAGTCCTC TCTCTTGAA GAGGACTGTGTTGCTACGG GGG 3′.

shRNA vectors were linearized by ScaI and electroporated into ESCs using a Bio-Rad gene pulser. Cells were selected in G418 (0.18 mg/ml) 24 h after electroporation for 5 days. Individual colonies were picked and PTIP levels were determined by western blotting. The PGK-Cre plasmid was electroporated into *Ptip* shRNA knockdown cells (20 ug DNA for 1 × 107 cells). Thirty-six hours after electroporation, HAT (hypoxanthine–aminopterin–thymidine) selection was performed for 5 days, after which cells were switched to HT (hypoxanthine–thymidine) media for 2 days and then transferred to normal media. Colonies were picked when visible, genomic DNA was extracted and Southern blotting was performed as described previously[17]. For PCR genotyping, the following primers were used to amplify the *Brca2* cko allele and *Brca2*-KO allele: *Brca2*-KO forward, 5′ GCCACCTCTGCCTGATTCTA; *Brca2*-KO reverse, 5′ AAAGAACCAGCTGGGGCTCGAG; *Brca2*-flox forward, 5′ TGAAGTGGACCCTGTAACCC; *Brca2*-flox reverse, 5′ AGTTCTCTCCTTTCAGC CTTCT.

Gene targeting and the gene conversion HR assay.

For gene targeting, ESCs were electroporated with 75 ug of linear targeting fragment from p59xDR–GFP[36], followed by selection for 5 days in 110 ug/ml hygromycin; then they were allowed to grow in normal ESC media[36]. Colonies were picked, and targeted clones were identified by Southern hybridization as described[36]. For the DSB-induced HR assay, ESCs were transiently electroporated with 20 ug of either pDR–GFP only or pDR–GFP plus I-SceI expressing vectors for 48 h. Gene conversion was read-out as the percentage of GFP-positive cells by flow cytometry analysis[41].

DNA fibre analysis.

Asynchronous B cells, *Brca2*-mutated PEO1 cells and *Brca2*-deficient K2BP tumors were labelled with 30 µM CldU, washed with PBS and exposed to 250 µM IdU. After exposure to IdU, the cells were washed again in warm PBS and treated or not with HU before collection. Cells were then lysed and DNA fibres stretched onto glass slides, as described[42]. The fibres were denatured with 2.5 M HCl for 1 h, washed with PBS and blocked with 2% BSA in phosphate buffered saline Tween-20 for 30 min. The newly replicated CldU and IdU tracts were revealed with anti-BrdU antibodies recognizing CldU and IdU respectively. Images were taken at 60 × magnification (Zeiss Axio Observer.Z1), and statistical analysis was performed using GraphPad Prism.

DSB detection by PFGE.

DSB detection by PFGE was done as described[42]. Ethidium-bromide-stained gels were analysed using an UVP EC3 imaging system. Quantification was performed using ImageJ normalizing DSB signals to unsaturated DNA signals in the well. Relative DSB levels were obtained by comparing treatment results to the background DSB signals observed for untreated conditions.

Western blotting and immunofluorescence.

Primary antibodies were used at the following dilutions: anti-tubulin (1:15,000, Sigma), anti-H3K4me3 (1:5,000, Millipore), anti-H3K4me1 (1:5,000, Millipore), anti-RAD51 (1:50, Santa Cruz), anti-PCNA (1:2,000, Santa Cruz), anti-total H3 (1:1,000 Millipore) and anti-Mre11 (1:10,000, gift from J. Petrini, MSKCC). MEFs were prepared for immunofluorescence by growth on 18 mm × 18 mm glass cover slips. Lymphocytes were dropped onto slides coated with CellTak (BD Biosciences). Cells were fixed with methanol and incubated with primary antibody as indicated.

iPOND and flow cytometry.

iPOND was performed essentially as described[22]. One hundred and fifty million WT, *Ptip*$^{-/-}$ and *Mll3*$^{-/-}$*Mll4*$^{-/-}$ MEFs were labelled with 10 μM EdU (Life Technologies) and treated with HU as indicated. Two hundred million cells were used for iPOND experiments with ESCs. Cells were cross-linked with 1% formaldehyde for 10 min at room temperature, quenched with 0.125 M glycine and washed with PBS. For the conjugation of EdU with biotin azide, cells were permeabilized with 0.25% Triton X-100/ PBS, and incubated in click reaction buffer (10 mM sodium-l-ascorbate, 20 μM biotin azide (Life Technologies), and 2 mM CuSO4) for 2 h at room temperature. Cells were resuspended in lysis buffer (50 mM Tris-HCl, pH 8.0, and 1% SDS) supplemented with protease inhibitors (Roche), and chromatin was solubilized by sonication in a Bioruptor (Diagenode-Pico) at 4°C for 24 min. After centrifugation, clarified supernatants were incubated for 1 h with streptavidin-MyOne C1 beads (Life Technologies). Beads were washed and captured proteins were eluted by boiling beads in 2 × NuPAGE LDS Sample Buffer (Life Technologies) containing 200 mM DTT for 40 min at 95 °C. Proteins were resolved by electrophoresis using NuPAGE Novex 4–12% Bis-Tris gels and detected by western blotting with the indicated antibodies. For flow cytometric analysis, asynchronous B cells were pulsed with 10 mM EdU for 20 min at 37 °C and stained using the Click-IT EdU Alexa Fluor 488 Flow Cytometry Assay Kit according to the manufacturer's specifications (ThermoFisher C-10425).

Generation of AZD2461-resistant KB2P tumors and in situ RAD51 assay.

Brca2$^{-/-}$*;p53*$^{-/-}$ mammary tumors were generated in *K14Cre;Brca2*$^{f/f}$*; p53*$^{f/f}$ (KB2P) female mice and genotyped as described previously[33]. Orthotopic transplantations into WT FVB/N/OLA (F1) mice, tumor monitoring, and sampling were conducted as described[43]. Starting from 2 weeks after transplantation, tumor size was monitored at least three times a week. All treatments were started when tumors reached a size of approximately 200 mm3. AZD2461 (100 mg/kg) was given orally for 28 consecutive days. If tumors did not shrink below 100% of the initial volume, treatment was continued for another 28 days. AZD2461 was diluted in 0.5% w/v hydroxypropyl methylcellulose in deionized water to a concentration of 10 mg/ml. For testing cross-resistance, mice were given a single treatment regimen of topotecan (2 mg/kg intraperitoneally, days 0–4 and 14–18) or cisplatin (Mayne Pharma, 6 mg/kg intravenously, day 0). Statistical analysis was performed using GraphPad Prism (log-rank Mantel–Cox test). The in situ RAD51 irradiation induced formation assay has been described[44].

Statistics.

Statistics was performed by two-tailed *t*-test, Mann–Whitney *U* test or by log-rank Mantel–Cox test unless otherwise specified. Statistical tests were justified appropriate for every figure. The data were normally distributed and the variance between groups being statistically compared was similar. No statistical methods or criteria were used to estimate sample size or to include/exclude samples. The investigators were not blinded to the group allocation during the experiments; however, the samples were coded before analysis unless otherwise specified.

36. Moynahan, M. E., Pierce, A. J. & Jasin, M. BRCA2 is required for homology-directed repair of chromosomal breaks. *Mol. Cell*. **7**, 263–272 (2001).

37. Ward, I. M. *et al.* 53BP1 is required for class switch recombination. *J. Cell Biol.* **165**, 459–464 (2004).

38. Lee, J. E. *et al.* H3K4 mono- and di-methyltransferase MLL4 is required for enhancer activation during cell differentiation. *eLife* **2**, e01503 (2013).

39. Cho, Y. W. *et al.* Histone methylation regulator PTIP is required for PPARγ and C/EBPα expression and adipogenesis. *Cell Metab.* **10**, 27–39 (2009).

40. Liu, W. *et al.* A selective small molecule DNA2 inhibitor for sensitization of human cancer cells to chemotherapy. *EBioMedicine* **6**, 73–86 (2016).

41. Pierce, A. J., Johnson, R. D., Thompson, L. H. & Jasin, M. XRCC3 promotes homology-directed repair of DNA damage in mammalian cells. *Genes Dev*. **13**, 2633–2638 (1999).

42. Ray Chaudhuri, A. *et al.* Topoisomerase I poisoning results in PARP-mediated replication fork reversal. Nature Struct. *Mol. Biol*. **19**, 417–423 (2012).

43. Rottenberg, S. *et al.* Selective induction of chemotherapy resistance of mammary tumors in a conditional mouse model for hereditary breast cancer. *Proc. Natl Acad. Sci. USA* **104**, 12117–12122 (2007).

44. Xu, G. *et al.* REV7 counteracts DNA double-strand break resection and affects PARP inhibition. *Nature* **521**, 541–544 (2015).

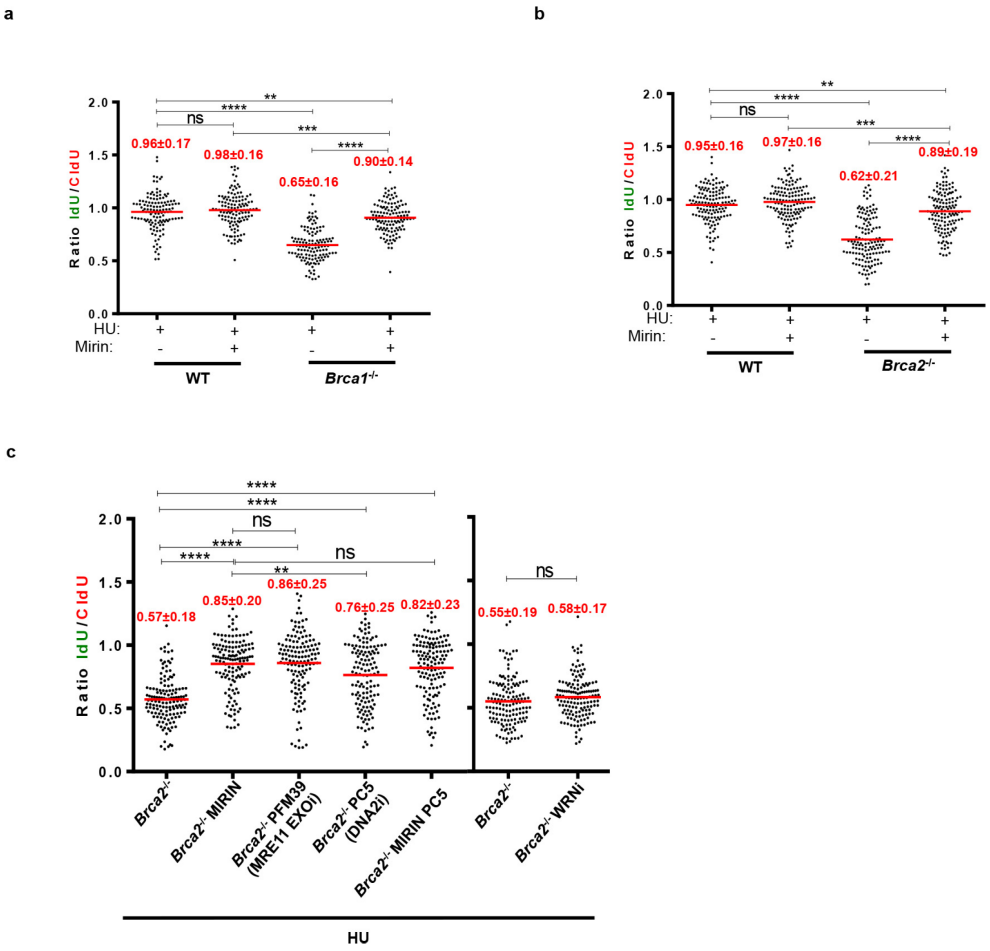

Supplementary Figure 1. Fork degradation in *Brca*-deficient B lymphocytes is mediated by MRE11 exonuclease activity. **a**, **b**, Ratio of IdU versus CldU upon HU treatment in WT, *Brca1*$^{-/-}$ (a) and WT, *Brca2*$^{-/-}$ (b) B lymphocytes with or without mirin pre-treatment. Numbers in red indicate the mean ± s.d. for each sample (**$P \leq 0.05$, ***$P \leq 0.001$, ****$P \leq 0.0001$, Mann–Whitney *U* test). One hundred and twenty-five replication forks were analysed for each genotype. **c**, Ratio of IdU versus CldU upon HU treatment in *Brca2*$^{-/-}$ B lymphocytes with or without mirin, PFM39 (MRE11 exonuclease inhibitor), PC5 (DNA2 inhibitor) or WRNi pre-treatment. Numbers in red indicate the mean ± s.d. for each sample (**$P \leq 0.05$, ****$P \leq 0.0001$, Mann–Whitney *U* test). One hundred and twenty-five replication forks were analysed for each genotype.

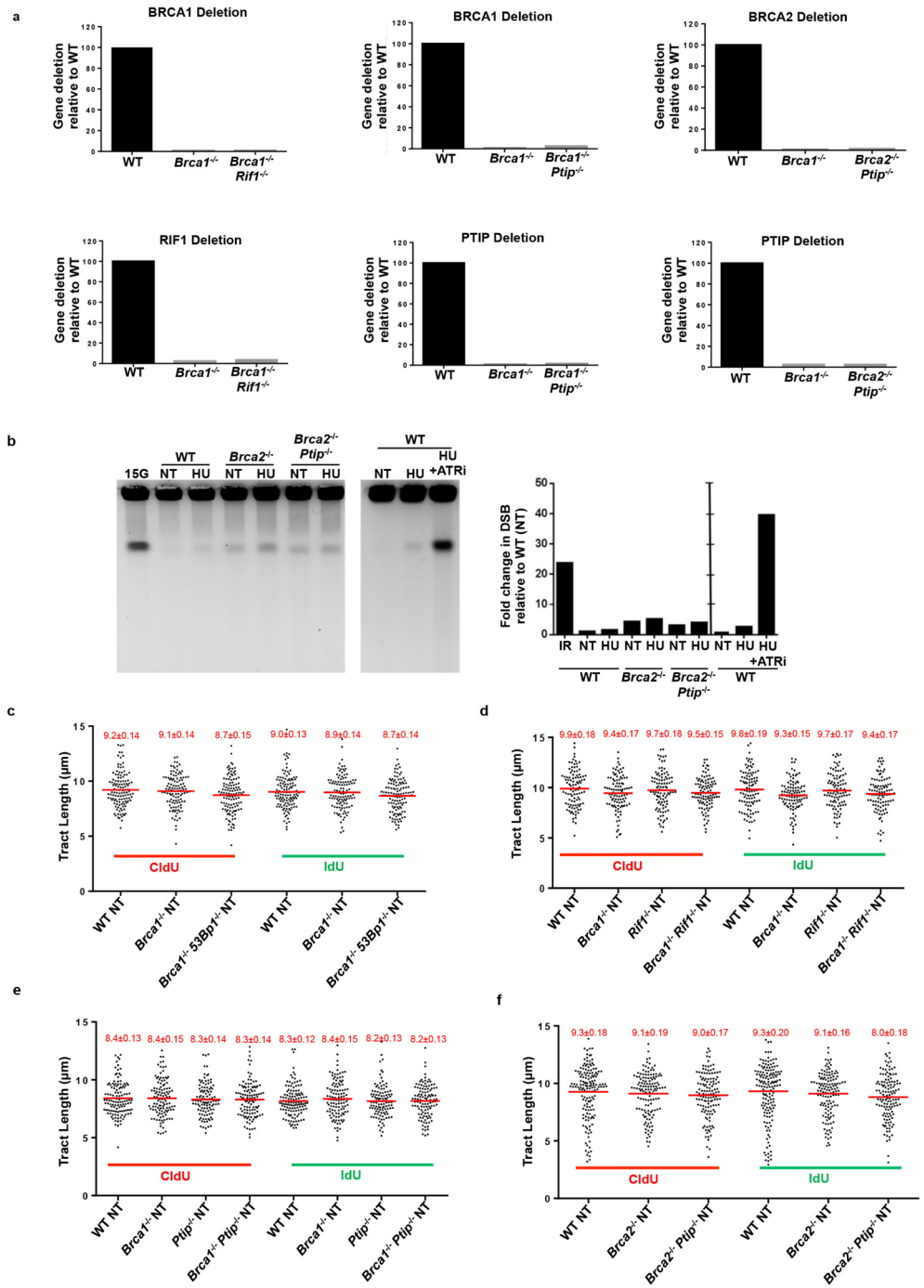
a
BRCA1 Deletion
BRCA1 Deletion
BRCA2 Deletion
RIF1 Deletion
PTIP Deletion
PTIP Deletion
Gene deletion relative to WT
WT
Brca1-/-
Brca1-/- Rif1-/-
Brca1-/- Ptip-/-
Brca2-/- Ptip-/-
b
15G
NT
HU
+ATRi
Fold change in DSB relative to WT (NT)
IR
c
d
e
f
Tract Length (μm)
CldU
IdU
WT NT
Brca1-/- NT
Brca1-/- 53Bp1-/- NT
Rif1-/- NT
Brca1-/- Rif1-/- NT
Ptip-/- NT
Brca1-/- Ptip-/- NT
Brca2-/- NT
Brca2-/- Ptip-/- NT

◀ **Supplementary Figure 2.** Replication fork progression rates and DSBs in B lymphocytes. **a**, Quantificative PCR analysis for *Brca1*, *Brca2, Ptip* and *Rif1* gene deletions in WT, *Brca1*$^{-/-}$, *Brca1*$^{-/-}$*Rif1*$^{-/-}$, *Brca1*$^{-/-}$*Ptip*$^{-/-}$, *Brca2*$^{-/-}$ and *Brca2*$^{-/-}$*Ptip*$^{-/-}$ primary B lymphocytes after infection with CRE. **b**, PFGE analysis for detection of DSBs in WT, *Brca2*$^{-/-}$ and *Brca2*$^{-/-}$*Ptip*$^{-/-}$ B lymphocytes treated with or without 4 mM HU for 3 h. Positive control for DSBs includes treatment of 15 Gy irradiation and HU +ATRi treatment for 3 h. Quantification of fold change in DSBs across genotypes relative to non-treated WT is plotted on the right. **c–f**, Replication fork progression rates, measured by tract lengths in micrometres, of CldU (red) and IdU (green) in WT, *Brca1*$^{-/-}$, *Brca1*$^{-/-}$*53bp1*$^{-/-}$, *Rif1*$^{-/-}$, *Brca1*$^{-/-}$*Rif1*$^{-/-}$, *Ptip*$^{-/-}$, *Brca1*$^{-/-}$*Ptip*$^{-/-}$, *Brca2*$^{-/-}$ and *Brca2*$^{-/-}$*Ptip*$^{-/-}$ primary B lymphocytes. Samples were not treated with HU. Numbers in red indicate the mean ± s.d. for each sample. One hundred and twenty-five replication forks were analysed for each genotype.

Supplementary Figure 3. Loss of PTIP rescues fork progression and restart defects in *Brca2*-deficient B lymphocytes but does not affect RAD51 IRIF. **a**, Genomic instability measured in metaphase spreads from B lymphocytes derived from WT, *Brca1*$^{-/-}$, *Rif1*$^{-/-}$, *Brca1*$^{-/-}$*Rif1*$^{-/-}$ mice treated for 6 h with 10 mM HU (*$P \leq 0.05$, unpaired *t*-test). Fifty metaphases were analysed per condition. Experiments were repeated three times. **b**, Genomic instability measured in metaphase spreads from B lymphocytes derived from WT, *Brca2*$^{-/-}$, *Ptip*$^{-/-}$, *Brca2*$^{-/-}$*Ptip*$^{-/-}$ mice treated for 6 h with 10 mM HU (*$P \leq 0.05$, unpaired *t*-test). Fifty metaphases were analysed per condition. Experiments were repeated three times. **c**, Fork progression in B lymphocytes derived from WT, Brca2$^{-/-}$, Ptip$^{-/-}$, Brca2$^{-/-}$Ptip$^{-/-}$ mice treated for 1 h with 0.2 mM HU. The *y* axis represents the tract lengths in micrometres. Numbers in red indicate the mean ± s.d. for each sample (****$P \leq 0.0001$, Mann–Whitney *U* test). One hundred and fifty replication forks were analysed for each genotype. **d**, Percentage of restarted replication forks in WT, *Brca2*$^{-/-}$, *Ptip*$^{-/-}$, *Brca2*$^{-/-}$*Ptip*$^{-/-}$ B cells treated for 1 h with 1 mM HU followed by 90 min recovery. Two hundred replication forks were analysed for each genotype. **e**, Tract lengths of restarted replication forks in WT, *Brca2*$^{-/-}$, *Ptip*$^{-/-}$, *Brca2*$^{-/-}$*Ptip*$^{-/-}$ B cells treated for 1 h with 1 mM HU followed by 90 min recovery. The *y* axis represents the tract lengths in micrometres. Numbers in red indicate the mean ± s.d. for each sample (NS, not significant, ****$P \leq 0.0001$, Mann–Whitney *U* test). One hundred and fifty replication forks were analysed for each genotype. **f**, Western blot analysis for RAD51 levels in WT, Ptip−/−, Brca2−/− and Brca2−/−Ptip−/− B cell extracts. Tubulin was used as loading control. **g**, Quantification of RAD51 foci formation in WT, *Brca2*$^{-/-}$, *Brca2*$^{-/-}$*Ptip*$^{-/-}$ B cells upon treatment with 5 and 10 Gy irradiation and recovery for 2, 4 and 6 h (*n* = 150 cells analysed).

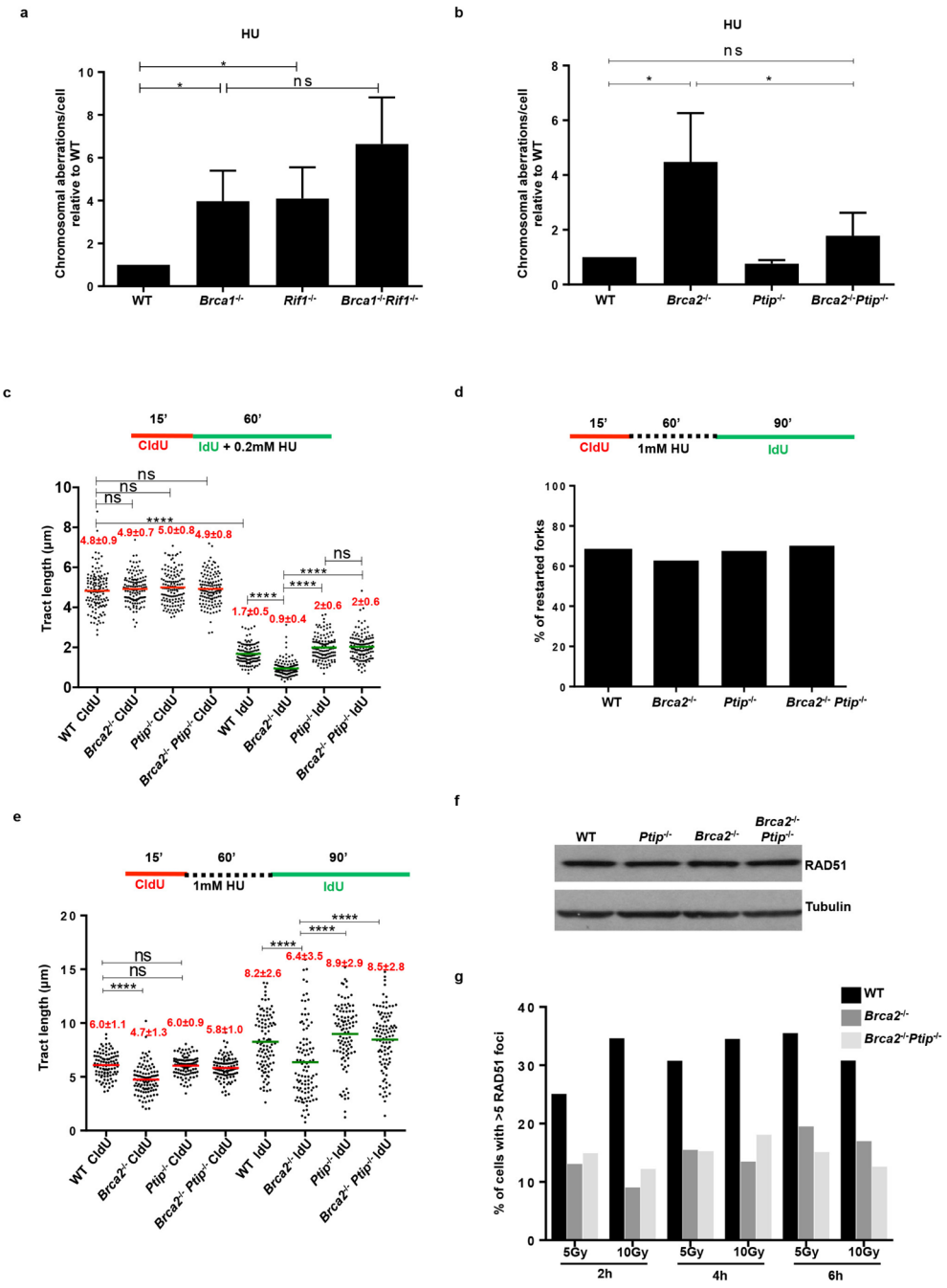
a
HU
Chromosomal aberrations/cell relative to WT
WT
Brca1-/-
Rif1-/-
Brca1-/-Rif1-/-
b
HU
Chromosomal aberrations/cell relative to WT
WT
Brca2-/-
Ptip-/-
Brca2-/-Ptip-/-
c
15'
60'
CldU
IdU + 0.2mM HU
Tract length (µm)
4.8±0.9
4.9±0.7
5.0±0.8
4.9±0.8
1.7±0.5
0.9±0.4
2±0.6
2±0.6
WT CldU
Brca2-/- CldU
Ptip-/- CldU
Brca2-/- Ptip-/- CldU
WT IdU
Brca2-/- IdU
Ptip-/- IdU
Brca2-/- Ptip-/- IdU
d
15'
60'
90'
CldU
1mM HU
IdU
% of restarted forks
WT
Brca2-/-
Ptip-/-
Brca2-/- Ptip-/-
e
15'
60'
90'
CldU
1mM HU
IdU
Tract length (µm)
6.0±1.1
4.7±1.3
6.0±0.9
5.8±1.0
8.2±2.6
6.4±3.5
8.9±2.9
8.5±2.8
f
WT
Ptip-/-
Brca2-/-
Brca2-/- Ptip-/-
RAD51
Tubulin
g
% of cells with >5 RAD51 foci
WT
Brca2-/-
Brca2-/-Ptip-/-
5Gy
10Gy
2h
4h
6h

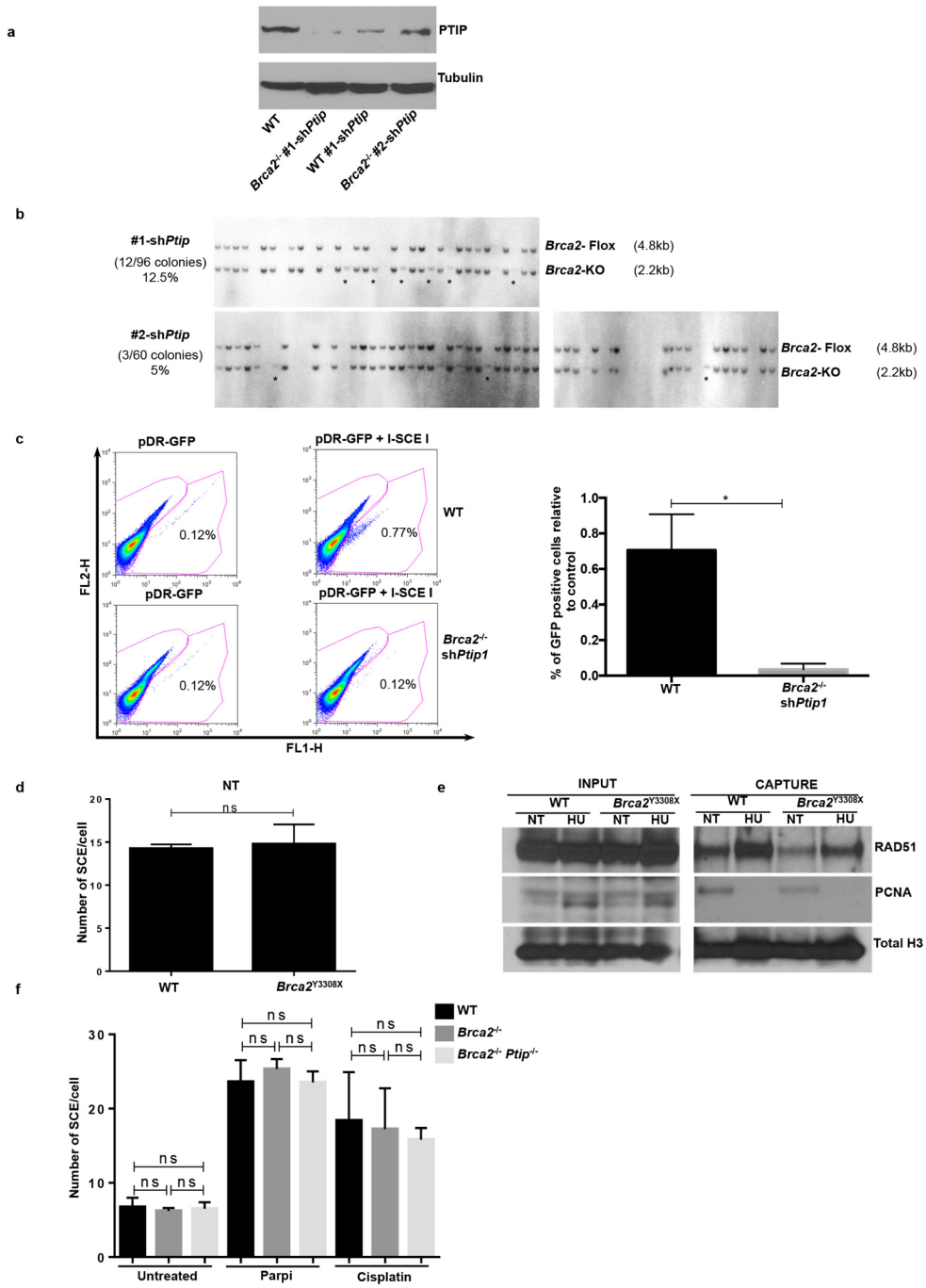
a
PTIP
Tubulin
WT
Brca2-/- #1-shPtip
WT #1-shPtip
Brca2-/- #2-shPtip
b
#1-shPtip
(12/96 colonies)
12.5%
Brca2- Flox (4.8kb)
Brca2-KO (2.2kb)
#2-shPtip
(3/60 colonies)
5%
Brca2- Flox (4.8kb)
Brca2-KO (2.2kb)
c
pDR-GFP
pDR-GFP + I-SCE I
0.12%
0.77%
0.12%
0.12%
WT
Brca2-/- shPtip1
FL2-H
FL1-H
% of GFP positive cells relative to control
WT
Brca2-/- shPtip1
d
NT
ns
Number of SCE/cell
WT
Brca2Y3308X
e
INPUT
CAPTURE
WT
Brca2Y3308X
NT
HU
RAD51
PCNA
Total H3
f
WT
Brca2-/-
Brca2-/- Ptip-/-
Number of SCE/cell
ns
Untreated
Parpi
Cisplatin

◀ **Supplementary Figure 4.** Depletion of PTIP rescues the lethality of *Brca2*-deficient ESCs. **a**, Western blot analysis for PTIP levels in WT and two different clones of *Brca2*$^{-/-}$ ESCs electroporated with shPtip. **b**, Southern blot analysis for determination of *Brca2* deletion in surviving clones electroporated with shPtip. Probes distinguishing the *Brca2*-flox allele (4.8 kb) (upper band) and *Brca2* KO allele (2.2 kb) (lower band) were used. *Surviving ESC clones with *Brca2* deletion and simultaneous downregulation of PTIP (12/96 *Brca2*-deleted colonies were found with shPtip1 and 3/60 colonies were found with shPtip2). Genotyping was confirmed by PCR (Fig. 2b). **c**, Top, representative FACS profiles of WT and *Brca2*$^{-/-}$/shPtip ESCs electroporated with either pDR–GFP plasmid only (control) or pDRGFP and I-SceI expressing vector for 48 h. Gene conversion of the pDR–GFP construct by HR is determined by the percentage of GFP-positive cells (FL1, green-detection filter; FL2, red-detection filter). Bottom, quantification of the percentage of GFP-positive cells in WT and *Brca2*$^{-/-}$/shPtip ESCs across three independent experiments. NS, not significant, *$P \leq 0.05$, unpaired *t*-test. **d**, Sister chromatid exchange (SCE) analysis in WT and Brca2^{Y3308X} hypomorphic ESCs. Twenty metaphases were analysed per condition; experiments were repeated three times. **e**, WT and Brca2^{Y3308X} hypomorphic ESCs were preincubated with mirin, EdU-labelled for 15 min and treated with 4 mM HU for 2 h. Proteins associated with replication forks were isolated by iPOND and detected by western blotting with the indicated antibodies. **f**, SCEs in WT, *Brca2*$^{-/-}$ and *Brca2*$^{-/-}$*Ptip*$^{-/-}$ B cells either untreated or treated overnight with 1 μM PARPi or with 0.5 μM cisplatin (NS, not significant, *$P \leq 0.05$, **$P \leq 0.001$, unpaired *t*-test). Twenty metaphases were analysed per condition; experiments were repeated three times.

Supplementary Figure 5. PTIP localizes to sites to DNA replication independently of DSBs. **a**, WT and *53bp1*$^{-/-}$ MEFs were retrovirally infected with a GFP-tagged PTIP construct. Cells were then irradiated with 10 Gy and allowed to recover. Co-localization of γ-H2AX (red) and PTIP (green) was assessed. Adjoining graph quantifies the percentage of cells with γ-H2AX foci co-localizing with PTIP upon irradiation (*n* = 150 cells analysed). Experiments were repeated three times. **b**, Western Blot analysis for endogenous and overexpressed PTIP levels in WT and *53bp1*$^{-/-}$ MEFs retrovirally infected with a GFP-tagged PTIP construct (GFP–PTIP). **c**, Quantification of the percentage of pan-nuclear γ-H2AXpositive cells with PTIP foci in WT and *53bp1*$^{-/-}$ MEFs upon treatment with HU (related to Fig. 3a) (*n* = 150 cells analysed). Experiments were repeated three times. **d**, Quantification of the percentage of cells with PTIP foci co-localizing with PCNA in WT and *53bp1*$^{-/-}$ MEFs in late S phase (related to Fig. 3b) (*n* = 150 cells analysed). Experiments were repeated three times. **e**, Representative immunofluorescence images of PCNA and 53BP1 co-staining in irradiated WT cells (10 Gy) or in late S-phase sites. White arrows indicate that the few 53BP1 foci observed in late S-phase cells do not co-localize with PCNA (*n* = 50 cells analysed). Experiments were repeated three times. **f**, Representative immunofluorescence images of WT and *Ptip*$^{-/-}$ MEFs treated with 4 mM HU for 2 h and analysed for ssDNA (BrdU) and MRE11 co-localization. Bottom panels shows the quantification of BrdU-positive cells (left) and the percentage of MRE11 co-localization in BrdU-positive cells (right) upon HU treatment in WT and *Ptip*$^{-/-}$ MEFs. (*n* = 150 cells analysed). Experiments were repeated three times. **g**, Quantification of the percentage of cells with MRE11 foci co-localizing with γ-H2AX upon irradiation treatment (10 Gy) in WT and *Ptip*$^{-/-}$ MEFs (related to Fig. 3e) (*n* = 150 cells analysed). Experiments were repeated three times. **h**, Cell cycle profiles in WT and *Ptip*$^{-/-}$ MEFs as measured by the incorporation of EdU (*y* axis) vs. DAPI (*x* axis). **i**, iPOND coupled to SILAC Mass-Spectrometry analysis for PTIP, H4 and RPA enrichment at stalled forks in 293T cells upon 3 mM HU treatment for 10 min and 4 h. The *y* axes represent the relative abundance of the indicated proteins on a log2 scale.

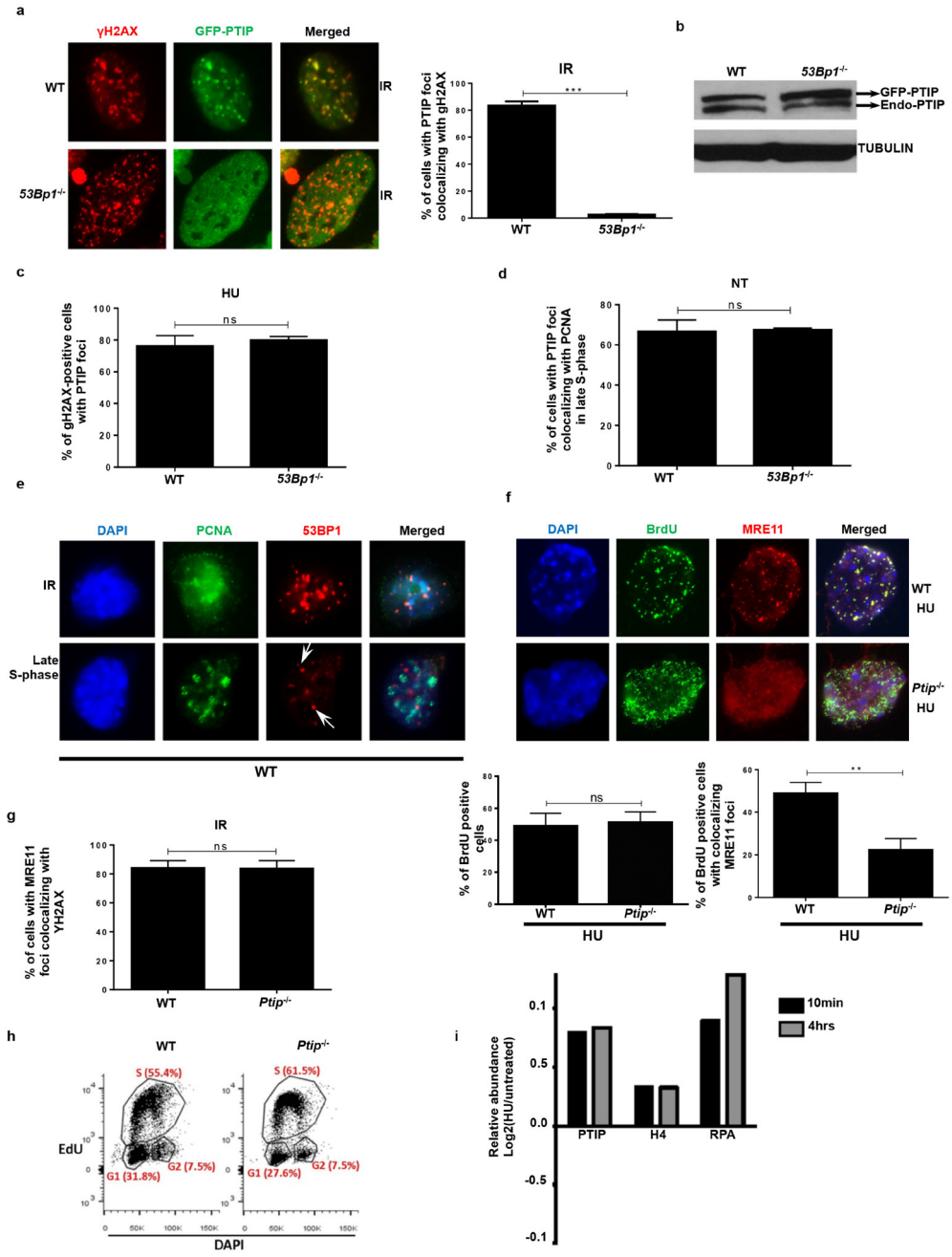
a
γH2AX
GFP-PTIP
Merged
WT
IR
53Bp1-/-
IR
IR
% of cells with PTIP foci colocalizing with gH2AX
***
WT
53Bp1-/-
b
WT
53Bp1-/-
GFP-PTIP
Endo-PTIP
TUBULIN
c
HU
% of gH2AX-positive cells with PTIP foci
ns
WT
53Bp1-/-
d
NT
% of cells with PTIP foci colocalizing with PCNA in late S-phase
ns
WT
53Bp1-/-
e
DAPI
PCNA
53BP1
Merged
IR
Late S-phase
WT
f
DAPI
BrdU
MRE11
Merged
WT HU
Ptip-/- HU
% of BrdU positive cells
ns
WT
Ptip-/-
HU
% of BrdU positive cells with colocalizing MRE11 foci
**
WT
Ptip-/-
HU
g
IR
% of cells with MRE11 foci colocalizing with YH2AX
ns
WT
Ptip-/-
h
WT
Ptip-/-
S (55.4%)
G2 (7.5%)
G1 (31.8%)
S (61.5%)
G2 (7.5%)
G1 (27.6%)
EdU
DAPI
i
Relative abundance Log2(HU/untreated)
10min
4hrs
PTIP
H4
RPA

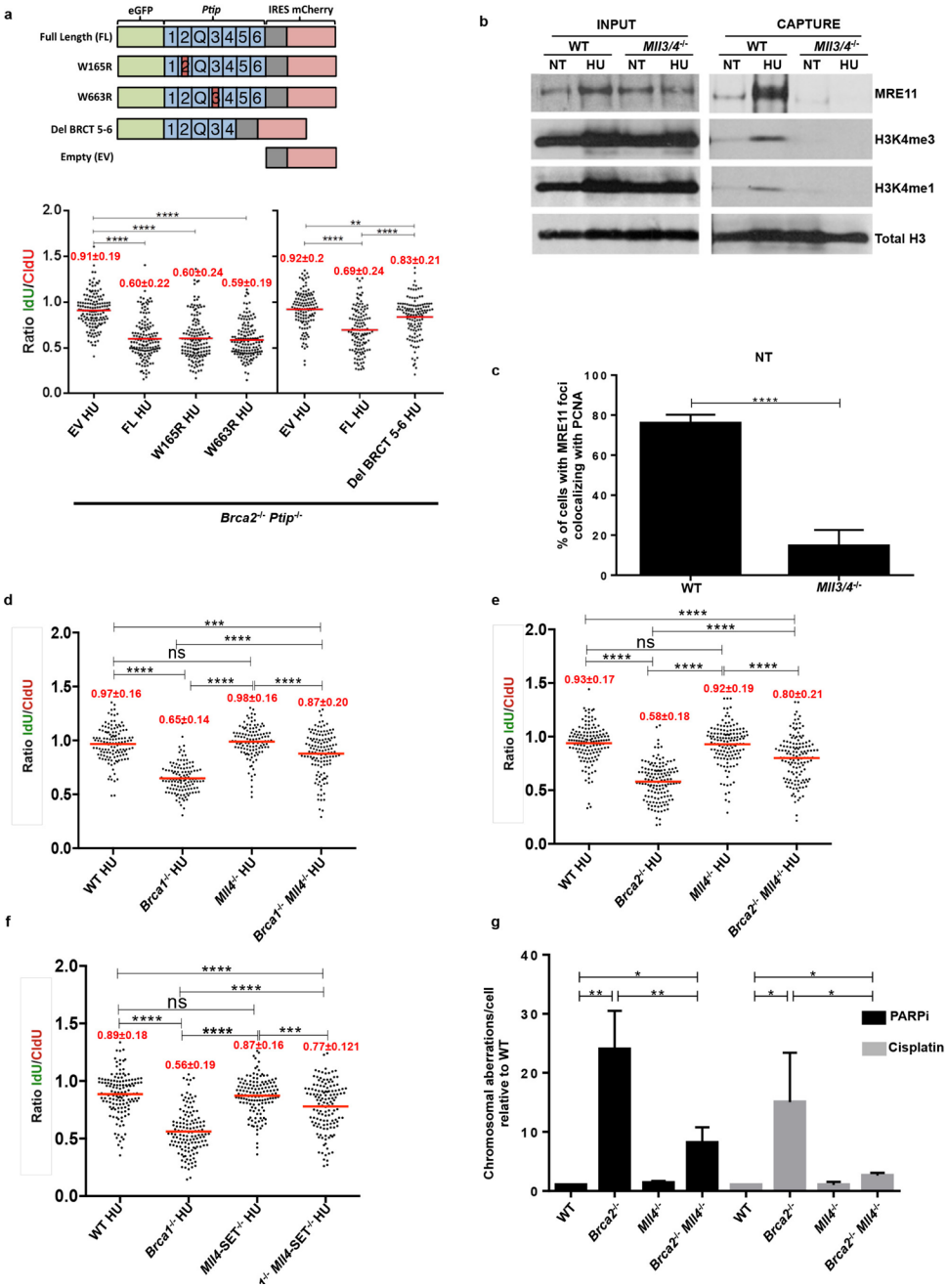
a
eGFP
Ptip
IRES mCherry
Full Length (FL)
W165R
W663R
Del BRCT 5-6
Empty (EV)
Ratio IdU/CldU
0.91±0.19
0.60±0.22
0.60±0.24
0.59±0.19
0.92±0.2
0.69±0.24
0.83±0.21
EV HU
FL HU
W165R HU
W663R HU
EV HU
FL HU
Del BRCT 5-6 HU
Brca2-/- Ptip-/-
b
INPUT
CAPTURE
WT
Mll3/4-/-
NT
HU
MRE11
H3K4me3
H3K4me1
Total H3
c
NT
% of cells with MRE11 foci colocalizing with PCNA
WT
Mll3/4-/-
d
Ratio IdU/CldU
0.97±0.16
0.65±0.14
0.98±0.16
0.87±0.20
WT HU
Brca1-/- HU
Mll4-/- HU
Brca1-/- Mll4-/- HU
e
Ratio IdU/CldU
0.93±0.17
0.58±0.18
0.92±0.19
0.80±0.21
WT HU
Brca2-/- HU
Mll4-/- HU
Brca2-/- Mll4-/- HU
f
Ratio IdU/CldU
0.89±0.18
0.56±0.19
0.87±0.16
0.77±0.121
WT HU
Brca1-/- HU
Mll4-SET-/- HU
-/- Mll4-SET-/- HU
g
Chromosomal aberrations/cell relative to WT
PARPi
Cisplatin
WT
Brca2-/-
Mll4-/-
Brca2-/- Mll4-/-
WT
Brca2-/-
Mll4-/-
Brca2-/- Mll4-/-

◀ **Supplementary Figure 6.** MLL3/4 promotes replication fork degradation in *Brca2*–deficient cells. **a**, Top, schematic of the retroviral PTIP mutant constructs used to identify the domain of PTIP involved in driving replication fork degradation. Different BRCT domains in PTIP are numbered and Q represents the glutamine rich region between the second and the third BRCT domains. Bottom, ratio of IdU versus CldU upon HU treatment of *Brca2*$^{-/-}$*Ptip*$^{-/-}$ B lymphocytes retrovirally infected with either EV, FL, W165R, W663R and Del BRCT 5-6 PTIP-mutant constructs and sorted for GFP or mCherry expression. Numbers in red indicate the mean ± s.d. for each sample (**$P \leq 0.01$, ****$P \leq 0.0001$, Mann–Whitney *U* test). One hundred and twenty-five replication forks were analysed for each condition. b, WT and *Mll3/4*$^{-/-}$ MEFs were EdU-labelled for 15 min and treated with 4 mM HU for 4 h. Proteins associated with replication forks were isolated by iPOND and detected by western blotting with the indicated antibodies. **c**, Quantification of the percentage of cells with MRE11 foci co-localizing with PCNA in late S phase in WT and *MLL3/4*$^{-/-}$ MEFs (*n* = 150 cells analysed). Experiments were repeated three times. **d–f**, Ratio of IdU versus CldU upon HU treatment in WT, *Brca1*$^{-/-}$, *Brca2*$^{-/-}$*Mll4*$^{-/-}$, *Mll4*-SET$^{-/-}$, *Brca1*$^{-/-}$*Mll4*$^{-/-}$, *Brca2*$^{-/-}$*Mll4*$^{-/-}$ and *Brca1*$^{-/-}$*Mll4*-SET$^{-/-}$ B cells. Numbers in red indicate the mean ± s.d. for each sample (NS, not significant, ****$P \leq 0.0001$, Mann–Whitney *U* test). At least 125 replication forks were analysed for each genotype. **g**, Genomic instability measured in metaphase spreads from splenic B cells derived from WT, *Brca2*$^{-/-}$, *Mll4*$^{-/-}$, *Brca2*$^{-/-}$*Mll4*$^{-/-}$ B cells treated overnight with 1 μM PARPi or with 0.5 μM cisplatin (**$P \leq 0.01$, ***$P \leq 0.001$, unpaired *t*-test). Fifty metaphases were analysed per condition. Experiments were repeated three times.

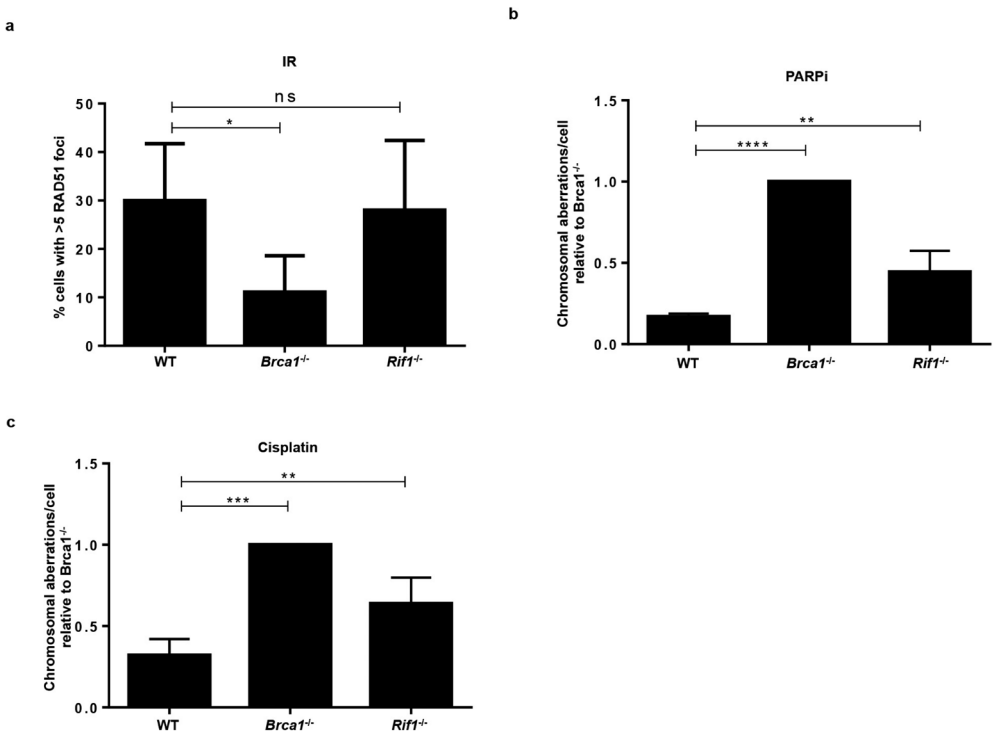

Supplementary Figure 7. Loss of RIF1 results in chromosomal instability. **a**, Quantification of RAD51 foci formation in WT, *Brca1*$^{-/-}$ and *Rif1*$^{-/-}$ B cells. Cells were treated with 10 Gy and harvested 4 h after irradiation (NS, not significant, *$P \leq 0.05$). At least 100 cells were analysed per condition; experiments were repeated three times. **b**, **c**, Genomic instability measured in metaphase spreads from splenic B cells derived from WT, *Brca1*$^{-/-}$ and *Rif1*$^{-/-}$ mice treated overnight with 1 μM PARPi (b) or with 0.5 μM cisplatin (c) (NS, not significant, **$P \leq 0.01$, ***$P \leq 0.001$, ****$P \leq 0.0001$, unpaired *t*-test). Fifty metaphases were analysed per condition; experiments were repeated three times.

Supplementary Figure 8. Multiple mutations can cause resistance to DNA-damaging agents in BRCA-deficient cells. **a**, **b**, Difference in progression-free survival (PFS) of *BRCA2*- and *BRCA1*-mutated ovarian serous adenocarcinoma patients with standard platinum-based regimens. Data were obtained from the TCGA project. Patients were separated into *PTIP* low- or high-expression on the basis of the 33rd percentile of *PTIP* expression z-scores. The difference between the PFS of PTIP-low versus PTIP-high was assessed by univariate log-rank P value ($P < 0.072$ and $P < 0.032$ in a and b, respectively). Analysis included 38 tumors with *BRCA1* mutations and 34 tumors with *BRCA2* mutations out of 316 high-grade serous ovarian cancers that underwent whole-exome sequencing. PFS curves for *PTIP*-low and *PTIP*-high expressing tumors were generated by the Kaplan–Meier method. All reported P values are two-sided. **c**, Western blot analysis for CHD4 and PTIP levels in PEO1 cells infected with shNSC and shCHD4. Tubulin was used as loading control. **d**, Cell cycle profiles in PEO1 cells infected with shNSC and shCHD4 as measured by the incorporation of EdU (*y* axis) versus DAPI (*x* axis). **e,** Immunostaining for MRE11 and PCNA in PEO1 cells infected with shNSC and shCHD4 upon treatment with 4 mM HU.

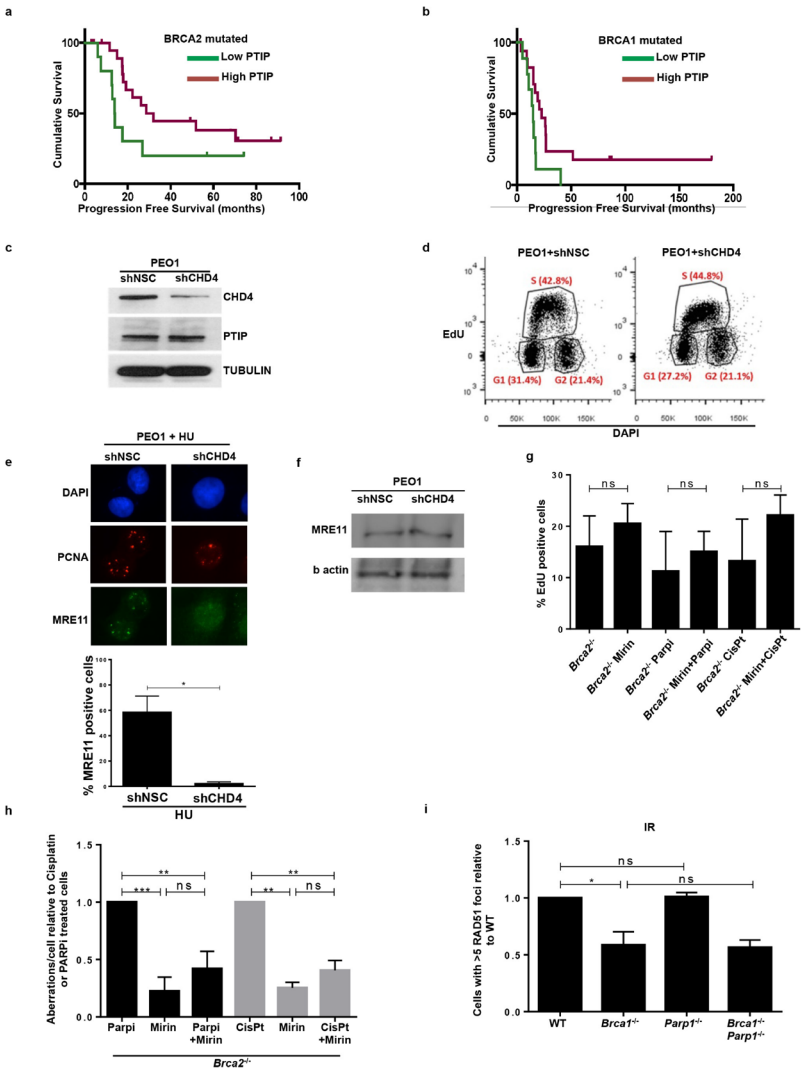

Bottom, quantification for MRE11 recruitment upon HU treatment. At least 100 cells were analysed per condition; experiments were repeated three times. **f**, Western blot analysis for CHD4 and MRE11 levels in PEO1 cells infected with shNSC and shCHD4. Actin was used as loading control. **g**, Percentage of EdU-positive cells was analysed 20 h after *Brca2*$^{-/-}$ B cells were treated with mirin alone, mirin+PARPi or mirin+cisplatin (NS, not significant). EdU was pulsed for 20 min before FACS analysis. Experiments were repeated three times. **h**, Genomic instability measured in metaphase spreads from B cells derived from *Brca2*$^{-/-}$ mice pretreated with 25 μM mirin for 2 h followed by overnight treatment with 1 μM PARPi or 0.5 μM cisplatin (NS, not significant, **P* ≤ 0.05, ***P* ≤ 0.001, unpaired *t*-test). Fifty metaphases were analysed per condition. Experiments were repeated three times. **i**, Quantification of RAD51 foci formation in WT, *Brca1*$^{-/-}$, *Parp1*$^{-/-}$ and *Brca1*$^{-/-}$*Parp1*$^{-/-}$ B cells treated with 10 Gy irradiation and harvested 4 h after treatment. At least 100 cells were analysed per condition; experiments were repeated three times.

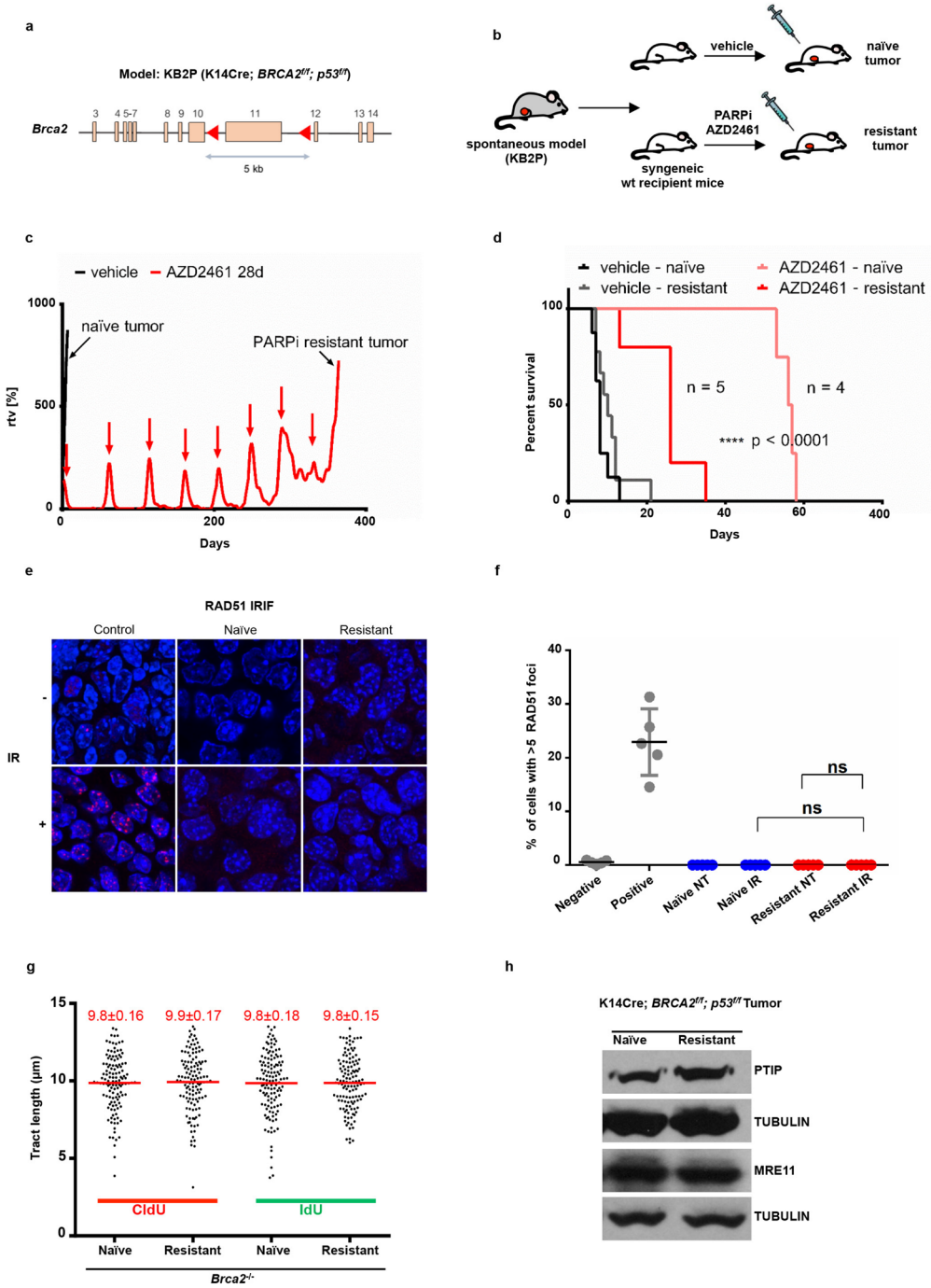
a
Model: KB2P (K14Cre; BRCA2f/f; p53f/f)
Brca2
3
4 5-7
8 9 10
11
12
13 14
5 kb
b
vehicle
naïve tumor
spontaneous model (KB2P)
PARPi AZD2461
resistant tumor
syngeneic wt recipient mice
c
vehicle
AZD2461 28d
naïve tumor
PARPi resistant tumor
rtv [%]
1000
500
0
0
200
400
Days
d
vehicle - naïve
vehicle - resistant
AZD2461 - naïve
AZD2461 - resistant
Percent survival
100
50
0
n = 5
n = 4
**** p < 0.0001
0
20
40
60
400
Days
e
RAD51 IRIF
Control
Naïve
Resistant
IR
-
+
f
% of cells with >5 RAD51 foci
40
30
20
10
0
ns
ns
Negative
Positive
Naïve NT
Naïve IR
Resistant NT
Resistant IR
g
Tract length (µm)
15
10
5
0
9.8±0.16
9.9±0.17
9.8±0.18
9.8±0.15
CldU
IdU
Naïve
Resistant
Naïve
Resistant
Brca2-/-
h
K14Cre; BRCA2f/f; p53f/f Tumor
Naïve
Resistant
PTIP
TUBULIN
MRE11
TUBULIN

◀ **Supplementary Figure 9.** *Brca2*-deficient tumors acquire PARPi resistance without restoration of RAD51 foci formation. **a**, Schematic depicting the conditional *Brca2* allele of the KB2P (*K14Cre;Brca2$^{f/f}$;p53$^{f/f}$*) spontaneous tumor model. **b**, Outline of the PARPi intervention study. A spontaneous BRCA2/p53-deficient tumor was generated and re-transplated into syngeneic WT mice. When the tumors reached 200 mm3, they were treated either with vehicle or PARPi AZD2461. **c**, PARPi response curve of the KB2P tumor (relative tumor volume (rtv) versus days). The treatment for 28 consecutive days was started when the tumor reached 200 mm3 (rtv = 100%). In response to the treatment, the tumor shrank but eventually grew back. When it reached 100% relative tumor volume, the treatment was repeated (as indicated with red arrows) for another 28 days. This regime was continued until the tumor became resistant to PARPi (black arrow). d, The stability of acquired resistance of the KB2P tumor was confirmed by re-transplanting matched naive and resistant tumors and treating animals either with vehicle or AZD2461 (only one 28-day cycle). Kaplan–Meier survival curve indicates that resistant tumors did not respond to the AZD2461 treatment, while naive tumors exhibited high sensitivity, indicative of a stable genetic mechanism of resistance. **e**, **f**, Irradiation-induced RAD51 foci were detected by immunofluorescence in the KB2P donor: RAD51 foci formation was undetectable in naive and resistant tumors, suggesting that HR restoration is not an underlying mechanism of PARPi resistance. Spontaneous tumors from *K14Cre; p53$^{f/f}$* (KP) mice treated with irradiation were used as positive control for RAD51 foci. Unirradiated KP cells were used as a negative control. **g**, Replication fork progression rates measured by tract lengths in micrometres of CldU (red) and IdU (green) in PARPi-naive or PARPi-resistant tumors. Numbers in red indicate the mean ± s.d. for each sample. One hundred and twenty-five replication forks were analysed for each condition. **h**, Western blot analysis for PTIP and MRE11 levels in PARPi-naive or PARPi-resistant tumors. Tubulin was used as loading control.

a

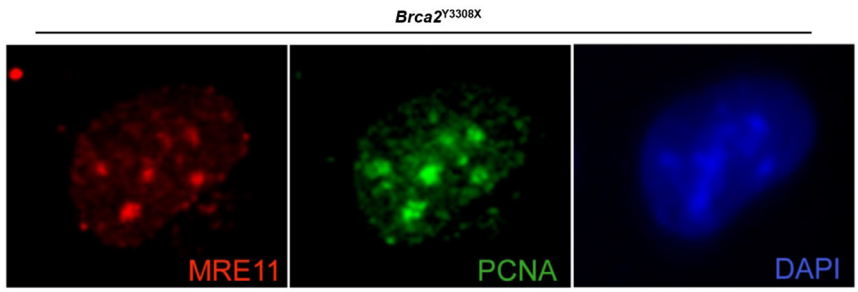

b

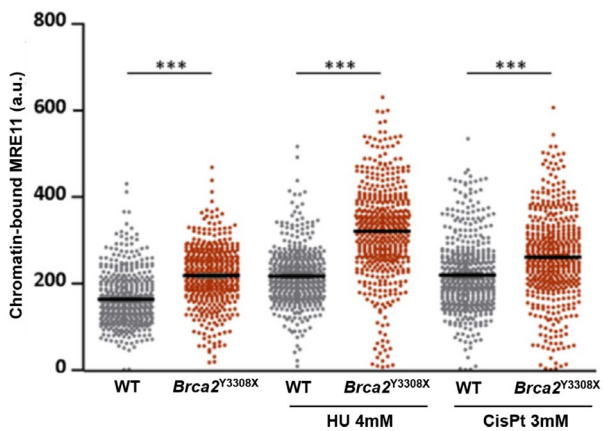

Supplementary Figure 10. *Brca2*-deficient ESCs have higher levels of chromatin-bound MRE11. **a**, Representative image of a Brca2 hypomorph mouse ESC (denoted *Brca2*^{Y3308X}) showing MRE11 foci (red) in S phase (identified by PCNA foci (green)). DNA was stained with DAPI (blue). **b**, High-throughput microscopy analysis quantifying the overall levels of chromatin-bound MRE11 per individual nucleus in WT and *Brca2*^{Y3308X} cells treated as indicated (a.u., arbitrary units).